

Shear viscosity and Stokes-Einstein violation in supercooled light and heavy water

Pierre Ragueneau, Frédéric Caupin,^{*} and Bruno Issenmann[†]

Institut Lumière Matière, Université de Lyon, Université Claude Bernard Lyon 1, CNRS, F-69622, Villeurbanne, France

(Dated: March 14, 2022)

We report shear viscosity of heavy water supercooled 33 K below its melting point, revealing a 15-fold increase compared to room temperature. We also confirm our previous data for the viscosity of supercooled light water, and reach a better accuracy. Our measurements, based on the spontaneous Brownian motion of 350 nm spheres, disagree at the lowest temperature with the only other available data, based on Poiseuille flow in a narrow capillary, which may have been biased by electro-osmotic effects. The viscosity ratio between the two isotopes reaches 2.2 at the lowest temperature. A companion Letter [F. Caupin, P. Ragueneau, and B. Issenmann, arXiv:2112.09010] discusses this giant dynamic isotopic effect. Here we provide a detailed description of the experiment and its analysis. We review the literature data about dynamic properties of water (viscosity, self-diffusion coefficient, and rotational correlation time), discuss their temperature dependence and compare their decoupling in the two isotopes.

I. INTRODUCTION

When a liquid can be measured during cooling to its glass transition temperature T_g , its shear viscosity is observed to increase tremendously, sometimes over more than 14 decades. One of the definitions of T_g is the temperature at which viscosity reaches 10^{12} Pa.s. The detailed temperature dependence of viscosity varies between liquids. Some, such as silica, exhibit a nearly Arrhenius behavior, whereas others, such as ortho-terphenyl, have a viscosity varying much faster than an Arrhenius law. The former are called strong liquids, and the latter fragile [1]. The glass transition is also characterized by heat capacity measurements. It is found that the relative temperature width of this calorimetric glass transition is large in strong liquids, and small in fragile ones [2].

Water shows a hybrid behavior. Although its viscosity can be measured over a relatively modest range due to crystallization above 230 K [3], available data shows a super-Arrhenius temperature dependence, typical of a fragile liquid. In contrast, the relative temperature width of its calorimetric glass transition (measured when heating low density amorphous ice) ranks water among the strongest liquids. This has led to the suggestion that water undergoes a fragile-to-strong transition [2], unfortunately lying in a temperature range not accessible to experiments.

Another puzzle with water as a glassformer is the early decoupling of its dynamic properties. Viscosity η , self-diffusion coefficient D_s , and rotational correlation time τ_θ (see Supplemental Material [4] for a definition of τ_θ and its discussion in the case of water) are usually tightly linked in liquids at high temperature, through the Stokes-Einstein (SE) and Stokes-Einstein-Debye (SED) relations, which respectively imply that $D_s\eta/T$ and $\eta/(T\tau_\theta)$

do not depend on temperature T . For usual fragile glassformers, $D_s\eta/T$ starts increasing when T decreases below around $1.3T_g$ [7]. In contrast, measurements on ortho-terphenyl have shown that $\eta/(T\tau_\theta)$ remains fairly constant over 14 decades of viscosity [8]. Water exhibits a qualitatively similar behavior, with a violation of the SE relation stronger than that of the SED relation [9]. However, the SE violation already starts at room temperature, more than $2T_g$.

To investigate further the SE and SED violations in water, accurate dynamic data in the supercooled region is needed. While available for D_s [10] and τ_θ [11], data for η is scarce. Two studies reported viscosity of deeply supercooled water [12, 13], but they disagree at the lowest temperatures. They were both based on Poiseuille flow, but used capillaries with very different diameters. This led us to perform measurements with an independent technique, using Brownian motion of spherical probes to obtain η without steady flow [9]. We could thus measure a 14-fold increase of viscosity from 293.15 to 239.15 K, and revealed a bias in the previous Poiseuille-flow study with the smallest capillary [13], which we attributed to electro-osmotic effects. Our data thus confirmed the fragile behaviour of water's viscosity, the early violation of the SE relation, and a milder violation of the SED relation [9].

Because the hydrogen bond, at the heart of water's anomalies, is strongly affected by isotopic substitution of hydrogen with deuterium [14], comparison between light and heavy water can provide new insight. Trading H_2O for D_2O represents a larger relative change in the moment of inertia of a molecule than in its mass. Therefore, one may expect that translational and rotational properties are affected in different ways. Unfortunately, whereas D_s [10] and τ_θ [11] data for supercooled D_2O are available, the only viscosity data is from Ref. [13], which we proved to be biased in the case of H_2O . It appears therefore necessary to produce reliable data for the viscosity of supercooled D_2O . To this end, we have applied the Brownian motion method to heavy water. We report here values down to 243.7 K, 33.3 K below the melting

^{*} frederic.caupin@univ-lyon1.fr

[†] bruno.issenmann@univ-lyon1.fr

point.

During this study, we were able to improve our measurement procedure, so that we also report new data for light water which agree with our previous results, but have better accuracy. Viscosity of supercooled water is a key parameter in the spreading of cold droplets on surfaces [15–17], making its precise knowledge relevant to the phenomenon of icing of roads and aircrafts.

The paper is organized as follows. Experimental details are presented in Section II and results in Section III. Section IV reviews the literature data on dynamic quantities of water (viscosity, self-diffusion coefficient and rotational correlation time). Their temperature dependence is analyzed in Section V, which also discusses the SE and SED violation. Concluding remarks are given in Section VI.

II. MATERIALS AND METHODS

A. Differential Dynamic Microscopy

To measure the viscosity of supercooled water, we use Differential Dynamic Microscopy (DDM) [18, 19] as described in Ref. [9]. In brief, monodisperse Brownian spheres (Duke Scientific, diameter $2r = 350$ nm) are dispersed in the liquid of interest. The samples are observed with a microscope (Zeiss Axioscope), equipped with a long working distance x100 objective (Mitutoyo M-Plan APO) and a CCD camera (Allied Vision Prosilica 1024×1024) with a frame rate up to 112 fps. The Brownian spheres are smaller than the resolution limit of the microscope, but scatter light when illuminated in transmitted light mode. As recommended in Ref. [18], the numerical aperture of the condenser is reduced to its minimum to decrease the incoherence parameter. Due to the temporal evolution of the light scattered by the colloids, the difference between two images taken at times t_1 and t_2 shows a granularity which increases with $|t_2 - t_1|$. Analysis of the spatial Fourier transform of image differences yields a decorrelation time τ as a function of wave vector modulus q . As explained in Refs. [18, 19] and shown in Fig. 1, for Brownian motion, $\tau = 1/(Dq^2)$, where D is the diffusion coefficient of the colloids.

The shear viscosity η follows from the Stokes-Einstein equation for a Brownian sphere:

$$\eta = \frac{k_B T}{6\pi r D}, \quad (1)$$

where k_B is the Boltzmann constant and T the temperature.

This technique is particularly suitable for measuring viscosity at deeply supercooled conditions, because it involves small volumes and does not induce strong perturbations in the fluid, such as steady flow or shear.

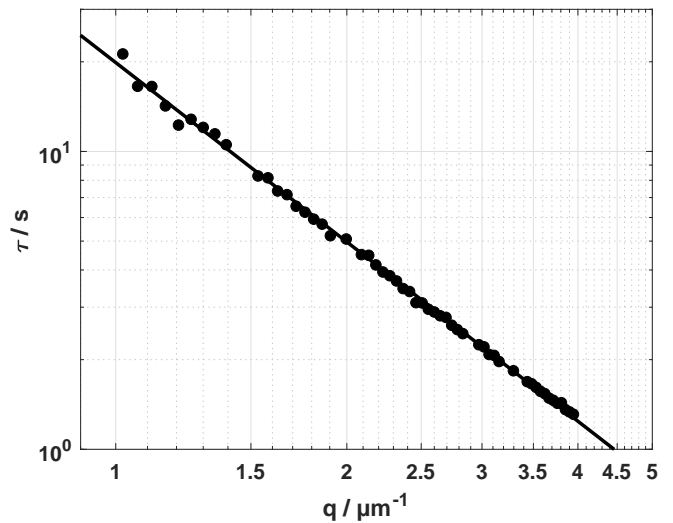


FIG. 1. Decorrelation time as a function of wave vector q in heavy water (mass fraction D_2O 97%) at -31°C . The line is a fit with $\tau = 1/(Dq^2)$, which yields $D = 5.03 \cdot 10^{-2} \mu\text{m}^2 \text{s}^{-1}$.

B. The colloidal suspension

1. H_2O suspension

The commercial colloidal suspension contains monodisperse polystyrene spheres suspended in water. To avoid the presence of possible contaminants like surfactants that could be included in the suspension, the suspension is first rinsed using the following procedure. First, the commercial suspension is diluted with ultrapure water (Direct-Q3, UV, Millipore) to obtain a 0.01% mass fraction of particles. Then 2 mL of the diluted suspension are centrifugated. The colloids fall at the bottom of the suspension and the supernatant liquid, including a large part of the possible contaminants, is removed with a pipette. Finally, ultrapure water is added to obtain a suspension with 0.01% mass fraction of colloids. The whole procedure is carried out twice.

2. D_2O suspension

The samples for the measurements of the viscosity of D_2O are prepared in a different way since the colloids are less dense than heavy water and cannot be centrifugated. To remove possible contaminants, the commercial suspension is diluted with ultrapure H_2O (to reach 0.1% mass fraction of colloids). This suspension is rinsed twice using the same procedure as above. Then it is centrifugated a third time and as much H_2O as possible is removed and replaced by D_2O ($\geq 99.9\%$, Eurisotop), to obtain a suspension whose mass fraction in colloids is 0.1%. Finally, this suspension is diluted ten times in D_2O to obtain the desired 0.01% mass fraction of particles.

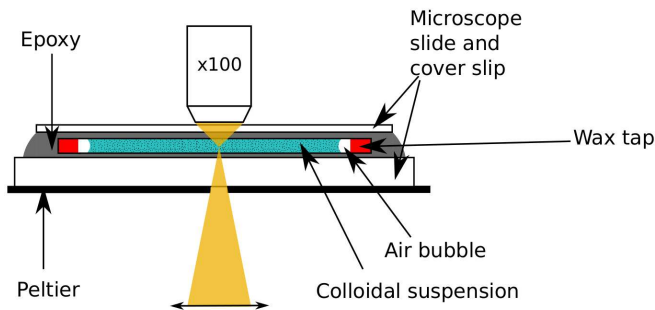


FIG. 2. Side view of the sample placed in the temperature-controlled stage of the microscope.

C. Experimental setup

1. Sample preparation

After rinsing, the suspension is placed in a borosilicate glass capillary with rectangular cross-section (Vitrotubes, internal dimensions $10 \times 0.2 \times 0.02$ mm, wall thickness around 0.01 mm). The capillary is then sealed by dipping its ends into fused wax (Hampton Research). Before sealing, we wait for evaporation of a quarter of the suspension, thus leaving air bubbles in order to avoid a pressure increase due to the expansion of water upon cooling. The sealed capillary is placed on a standard microscope slide (thickness 1 mm) together with two capillaries containing respectively pure water and pure dodecane for temperature calibration (see § IID 2). The three capillaries are covered with epoxy. Finally, a microscope cover slip is put on top of them and the sample is left drying for 15 minutes under a 230 g weight. Fig. 2 shows a sketch of the final setup. The temperature calibration capillaries are omitted in this figure for clarity. The sample is placed in a thermal stage (Linkam LTS120 Peltier system) to control its temperature down to 233K; silica gel is added in the stage chamber to avoid moisture condensation on the cold microscope cover slip. The thermal stage is fixed on the microscope for DDM measurement.

2. Acquisition parameters

DDM requires a fast enough acquisition to capture particle displacements of the order of their size between successive frames. As the mean square displacement of a Brownian particle during time t scales as \sqrt{Dt} , the acquisition frequency should scale as D , which is inversely proportional to the shear viscosity η (Eq. 1). Therefore, as a run is performed for a series of decreasing temperatures, corresponding to increasing η values, the frame rate fps of the camera is successively decreased as $\text{fps} \propto 1/\eta$, using an approximate extrapolated value of η for this calcula-

tion. Typical data consist of a sequence of 1500 square images (1024×1024 pixels), acquired at 10 – 112 fps depending on temperature, with 8 ms exposure time.

D. Temperature calibration

As the viscosity of water is a steep function of temperature in the supercooled region [9], it is critical to have an accurate value for the sample temperature, which might differ from the nominal temperature of the thermal stage. For example, complete melting of ultrapure ice is observed at a nominal temperature of $-0.3 \pm 0.1^\circ\text{C}$, which reveals the existence of temperature gradients across the sample. We found a negligible change in the melting point of ice when replacing the bottom microscope slide by a thinner one. Therefore, the temperature gradient is rather a lateral one, due to the hole in the center of the Peltier element, which allows illuminating the sample. We note that the quality of the thermal contact between the polished heating/cooling element of the stage, the microscope slide, and the capillaries may affect this temperature gradient. We checked this by measuring the melting point of water and undecane in around ten capillaries prepared as described in Section IIC 1. We found a dispersion of the melting temperatures lower than the reading resolution (0.1°C). This shows that immersing the capillaries in epoxy allows achieving a reproducible thermal contact and reducing temperature variability. In the remainder of this section, we describe how we calibrated the temperature in the observed section of the capillary using the melting point of pure chemicals.

1. Melting point determination of calibration chemicals

We selected a series of pure chemicals covering the temperature range of our experiments and measured their actual melting temperature $T_{m,\text{act}}$ as follows. $16 \mu\text{L}$ of the chemical are put in a Pasteur pipette, previously fused-welded at one end. A platinum resistor (Pt-100 Ω , 1/3 DIN, previously calibrated in melting ice) is immersed in the liquid and its resistance measured with a digital multimeter (Tektronix DMM4050) in 4-wires mode. The Pasteur pipette is immersed in a thermal bath (Julabo FP89-HL) whose temperature is lowered until complete crystallization of the chemical. Then the bath temperature is ramped up to room temperature. Figure 3 (inset) displays a typical temperature trace of the Pt-100 resistor, from which $T_{m,\text{act}}$ is obtained. The results for 4 chemicals are given in Table I.

2. Principle of the calibration with pure chemicals

To calibrate the temperature of the sample in the observed section of the capillary, we make the same samples

TABLE I. Melting points of the 4 chemicals used for temperature calibration (see text for details). Uncertainties correspond to a 68% confidence interval.

Chemical	Actual melting point $T_{m,act}$ ($^{\circ}\text{C}$)	Tabulated melting point [20] ($^{\circ}\text{C}$)	$T_{m,Linkam}$ ($^{\circ}\text{C}$)
Dodecene	-35.18 ± 0.02	-35.19	-36.6 ± 0.1
Undecane	-25.92 ± 0.06	-25.54	-26.8 ± 0.1
Ultrapure water	0	0	-0.4 ± 0.1
Heptadecane	21.1 ± 0.3	21.97	21.2 ± 0.1

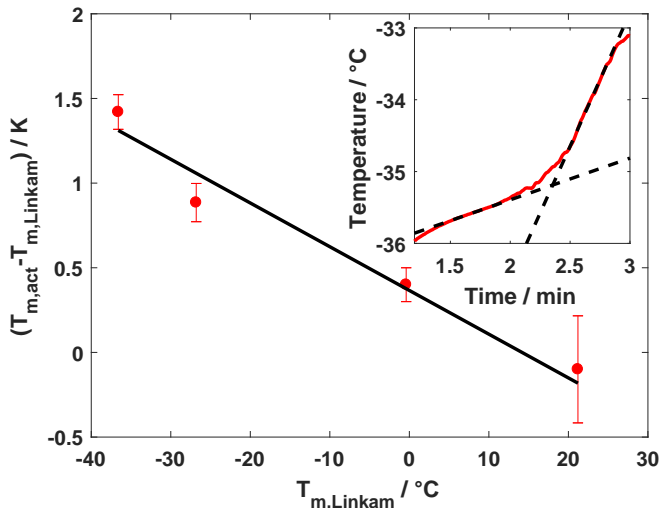


FIG. 3. $\Delta T = T_{m,act} - T_{m,Linkam}$ as a function of $T_{m,Linkam}$ for the 4 chemicals listed in Table I. The line is a linear least- χ^2 fit. Inset: Determination of the melting point of dodecene during heating in the thermal bath: $T_{m,act}$ is given by the intersection of the two straight lines.

as described above, only replacing the colloidal suspension inside the capillary by a pure chemical. After being placed in the thermal stage, the sample is cooled until it crystallizes. Then, by slow step-wise heating, we determine the nominal stage temperature $T_{m,Linkam}$ at which a crystal located at the center of the observation area grows or remains stable at $T_{m,Linkam} - 0.1$ K, while it completely melts at $T_{m,Linkam}$. The precision on $T_{m,Linkam}$ is $\pm 0.1^{\circ}\text{C}$. Comparison of this measurement with the actual melting temperature of the chemical provides a calibration of the thermal stage.

Figure 3 shows the difference $\Delta T = T_{m,act} - T_{m,Linkam}$ as a function of $T_{m,Linkam}$. In the temperature range of our experiment, ΔT is a linear function of $T_{m,Linkam}$. However, the exact function may vary with sample, for instance due to a change in room temperature or a different contact between the Peltier element and the microscope slide. To avoid this issue, we performed an *in situ* temperature calibration for each sample, thanks to the two capillaries added next to the capillary containing the colloidal suspension (see Section II C 1). One is filled with dodecene, and the other with ultrapure water. The measurement of the corresponding melting points just

after the DDM run allows a quick calibration of the linear relationship between ΔT and $T_{m,Linkam}$ for that run, thus giving accurate values for the sample temperatures during the run.

E. Isotopic fraction

An additional difficulty of the experiments with D_2O is isotopic purity. The sample can be contaminated by light water during preparation, due to isotopic exchange with ambient water vapor and to the light water present in the commercial colloidal solution. To minimize contamination, the heavy water bottle and prepared colloidal solution are stored in a nitrogen container. All sample preparations are performed under a steady nitrogen flux. Despite all these precautions, the D_2O fraction in the resulting sample was less than in the initial solution. The measured viscosity η is then the one of an isotopic mixture, whose D_2O mole fraction x needs to be determined.

We obtained x from the melting point of the mixture. After crystallization upon cooling, we warm up the sample in the stage until complete melting is observed under the microscope. The melting point T_m (in $^{\circ}\text{C}$) of D_2O - H_2O mixtures is $T_m = 4.213x - 0.411x^2$ [21]. The accuracy on T_m is around 0.15 K, resulting in an absolute accuracy of 0.04 on x . This measurement is performed at the end of a run, together with the temperature calibration, since crystallization of the solution leads to aggregation of the colloids. Typical values of x ranged from 0.47 to 0.97.

F. Viscosity calculation for H_2O

For each run, a reference diffusion coefficient is measured at $T_0 = 293.15$ K, where the viscosity of pure light water is known with the best accuracy and precision [22]: $\eta_0(T_0) = 1.0016 \pm 0.0017$ mPa.s. Here T_0 is the nominal temperature of the stage. At this temperature, the difference between T_0 and the actual one is small, and the viscosity has only a small temperature dependence, so that a correction of T_0 is not necessary.

DDM gives $D(T)$, the diffusion coefficient of the Brownian spheres as a function of temperature. To convert these values into viscosity $\eta_0(T)$ of water, we take the ratio of the Stokes-Einstein equations (Eq. 1) at tem-

perature T and at the reference temperature T_0 , which yields:

$$\eta_0(T) = \eta_0(T_0) \frac{T}{T_0} \frac{D(T_0)}{D(T)}. \quad (2)$$

As explained before [9], this relative measurement avoids possible effects of the capillary walls and of the electric double layer around the colloids on their diffusion coefficient. Knowledge of the sphere radius r is not needed, as it cancels out when taking the ratio of the Stokes-Einstein equations, because the expansion coefficient of polystyrene is negligible in this temperature range.

Viscosity values for H₂O are given for each run in the Supplementary Information. A run corresponds to one sample, containing a capillary with colloids suspended in water, and two capillaries containing respectively dodecene and pure water to calibrate *in situ* the temperature as described above. For most temperatures, the viscosity was measured several times (often 3).

In our previous work [9], $D(T_0)$ was measured in 12 independent samples which resulted in a 2.5% standard deviation. However, the standard deviation of $D(T_0)$ measured 10 times on the same sample is around 1.5% only. In the present work, to improve the precision of our data, we applied Eq. 2 to each sample by measuring $D(T_0)$ 10 times on this sample before performing experiments at other temperatures, instead of rescaling the data for different samples by the same reference measurement averaged on several samples. Therefore, we now take for the intrinsic relative uncertainty (1 SD) on η 1.5%. The temperature uncertainty δT also contributes to the uncertainty on viscosity. To take it into account, we first least-square fit the viscosity values by the Speedy-Angell law

$$\eta(T) = \eta_0 \left(\frac{T}{T_s} - 1 \right)^{-\gamma}, \quad (3)$$

and calculate the total relative uncertainty (1 SD) at temperature T as $\sqrt{(0.015)^2 + (\delta T \times \gamma / (T - T_s))^2}$. The resulting uncertainty ranges from 1.5% at the highest temperature to 2.2% at the lowest temperature.

G. Viscosity calculation for D₂O

Viscosity values for D₂O were calculated in the same way as for H₂O based on a reference viscosity $\eta(x, T_0)$ for each sample with D₂O mole fraction x , where $T_0 = 293.15$ K the same reference temperature as above. At T_0 , viscosity is well described by a linear relation [23]:

$$\eta(x, T_0) = (1 - x)\eta(0, T_0) + x\eta(1, T_0). \quad (4)$$

The viscosity $\eta(1, T_0)$ of heavy water at the reference temperature T_0 was measured by Millero [24]. Millero calibrated his measurements using the reference value for

TABLE II. $1 - \sigma$ relative uncertainties on the measurements of η_{D_2O} as a function of temperature.

Temperature range	$\frac{d\eta_{D_2O}(T)}{\eta_{D_2O}(T)}$ (%)
$T \geq 260$ K	2
$255 \text{ K} \leq T < 260$ K	3
$250 \text{ K} \leq T < 255$ K	4
$T < 250$ K	7

the viscosity of H₂O at T_0 known at that time, that was 1.0020 mPa.s. This reference value was since re-evaluated to $\eta(0, T_0) = 1.0016 \pm 0.0017$ mPa.s [22]. Therefore, we recalculated Millero's values and propagated the errors of Millero and $\eta(0, T_0)$ to obtain $\eta(1, T_0) = 1.2466 \pm 0.0021$ mPa.s.

The viscosity $\eta(x, T)$ of the sample are then calibrated using the reference value $\eta(x, T_0)$ in Eq. 2. We thus obtain viscosity values for the isotopic mixtures at each temperatures. To extrapolate the data to pure D₂O, we still need to check that the linear Eq. 4 remains valid far in the supercooled region. To do so, all the data were binned into 0.1 K intervals and fitted by

$$\eta(x, T) = x\eta(1, T) + a(1 - x). \quad (5)$$

Smoothed viscosity values for pure H₂O calculated from Eq. 3 with the best-fit parameters listed in table IV are included in the fitted data at all temperatures. The uncertainty on x is projected on the vertical axis and combined to the uncertainty on η .

The fitting parameters are a , which agrees well with the measured values of the viscosity of pure H₂O, and $\eta(1, T)$, which is thus taken as the viscosity of pure D₂O. Typical examples are displayed in Fig. 4, showing that the linear relation remains valid over the whole temperature range of our study.

As the sources of uncertainty in this measurement is more complex than in light water (in particular due to the uncertainty on the mass fraction x of heavy water), we could not use the same procedure to estimate the final uncertainty. We first least-square fit the raw data by a Speedy-Angell law (Fig. 5, bottom panel). The deviation of the experimental data from the fitting equation is shown in the top panel. It can be seen that the data scatter increases at low temperatures. To be conservative, 4 different temperature ranges were considered, and the relative uncertainty was calculated as the standard deviation of the data in each temperature range. The values are given in Table II.

III. RESULTS

A. Improved viscosity values for H₂O

Figure 6 displays the raw values of the viscosity of light water (listed in Supplementary Information) and

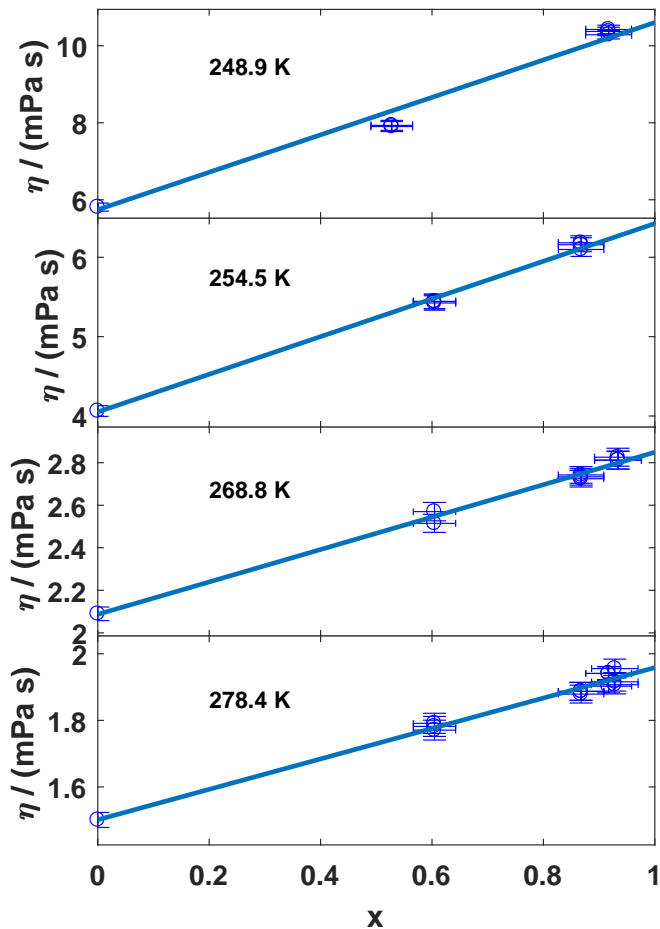


FIG. 4. Shear viscosity η as a function of D_2O molar fraction x for various temperatures (± 0.05 K). The lines are least- χ_2 fit with Eq. 5.

their least- χ_2 fit by a Speedy-Angell law with $\eta_0 = 0.13746$ mPa s, $T_s = 225.9151$ K and $\gamma = 1.6383$. The resulting smoothed values $\eta_{\text{smoothed},\text{H}_2\text{O}}(T)$ are given in Table XIV. The fit reduced residuals for individual measurements are also shown in the top panel of Fig. 6: they are consistent with our estimate of the measurement uncertainty (Section II F).

Figure 7 compares the present data to previously published data sets [9, 12, 13, 25–27]. We confirm with a better precision our previous results [9], and, as already explained therein, we confirm the agreement with Collings [26], Berstad [27], Hallet [12] and Eicher [25] (as corrected by Kestin [28]), except for a slight deviation from Hallet at the lowest temperatures. We confirm the large deviation with Osipov’s data [13] that we previously attributed to a possible electro-osmosis effect that could have biased their results [9].

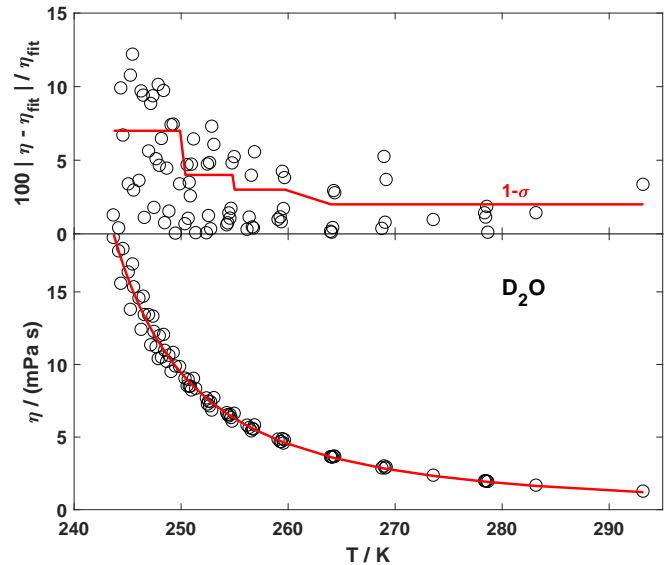


FIG. 5. Bottom panel: raw viscosity data for pure D_2O . The red curve is a least-square fit with the Speedy-Angell power-law (Eq. 3). Top panel: Relative deviation between data and fit. The $1 - \sigma$ relative uncertainty corresponds to a 68% confidence interval.

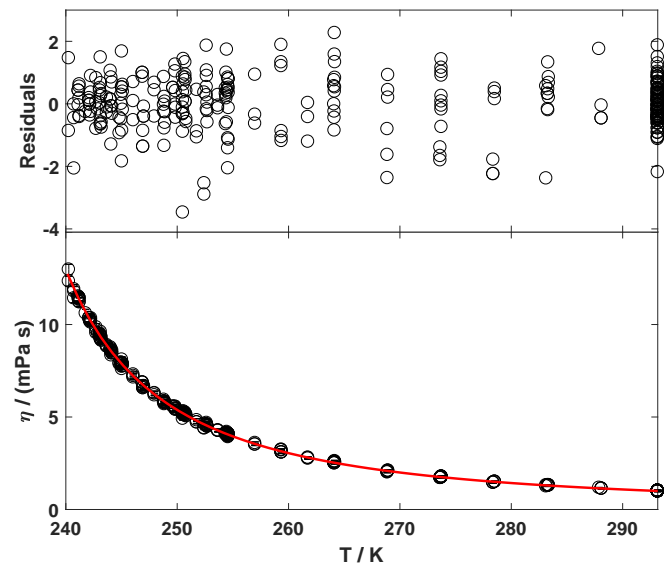


FIG. 6. Lower panel: viscosity of H_2O as a function of temperature. The red curve is $\eta_{\text{smoothed},\text{H}_2\text{O}}(T)$. Upper panel: reduced residuals $[\eta(T) - \eta_{\text{smoothed}}(T)] / \sigma(T)$.

B. Viscosity values for D_2O

Figure 5 displays raw viscosity values for D_2O (listed in the Supplementary Information). Using uncertainties from Table II, they are least- χ_2 fitted by a Speedy-Angell law, which yields the following best-fit parameters: $\eta_0 = 1.3212 \cdot 10^{-4}$ Pa.s, $T_s = 230.9681$ K and $\gamma = 1.7061$. The smoothed values $\eta_{\text{smoothed},\text{D}_2\text{O}}(T)$ calculated using this fit are given in Table XIV.

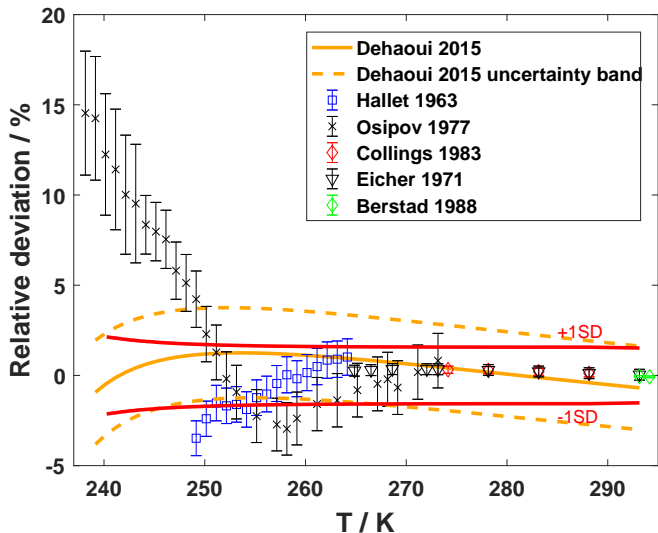


FIG. 7. Relative deviation of literature data [9, 12, 13, 25–27] from our results $\eta_{\text{smoothed},\text{H}_2\text{O}}$ (Table XIV). The curves show the uncertainty band (± 1 standard deviation) for our previous data [9] (dashed orange) and the present ones (solid red).

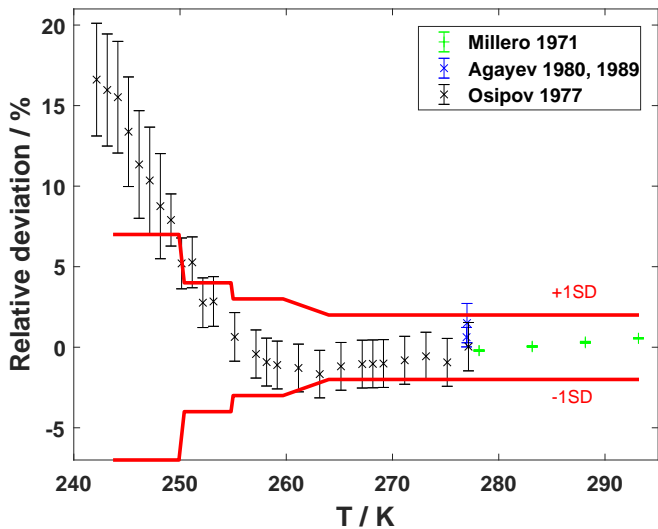


FIG. 8. Relative deviation of literature data [13, 24, 29, 30] from our results $\eta_{\text{smoothed},\text{D}_2\text{O}}$ (Table XIV). The red curves show the uncertainty band (± 1 standard deviation) of our measurements.

Figure 8 compares the present data to previously published data sets [13, 24, 29, 30]. Like in the case of light water, our data agree with Millero [24] and Agayev [29, 30], whereas they systematically deviate from Osipov’s data [13]. The deviation is however less striking than in the case of light water, due to the lower precision of our D_2O data.

IV. CHOICE OF LITERATURE DATA

To test the SE and SED relations, we need to combine our viscosity data together with previously tabulated viscosity data in the stable liquid, and then with data for the self-diffusion coefficient and the rotational correlation time. In this section we explain how the literature data were chosen.

A. Viscosity, self-diffusion and rotational correlation time of H_2O

The most accurate sources of viscosity data for H_2O are gathered in Table III. We used Eicher’s data as re-evaluated by Kestin [28]. Eicher’s, Colling’s, Korosi’s and Kestin’s (1985) data were recalculated using the current reference value for viscosity of pure light water at 293.15 K, $\eta(T_0) = 1.0016 \text{ mPa s}$ [22]. Kestin’s and Korosi’s data are measured under pressure, but below 20 bars. The weak pressure dependence of dynamic parameters allows neglecting the difference between those data and the atmospheric pressure value. Berstad’s data are calculated using the provided fits from 20 to 25°C every 1°C.

To generate SE and SED plots for H_2O , we combine individual viscosity data points with Speedy-Angell fits to self-diffusion and rotational correlation time:

$$A(T) = A_0 \left(\frac{T}{T_s} - 1 \right)^{-\gamma}. \quad (6)$$

The best-fit parameters for D_s and τ_θ were given previously [9]; for easy reference, they are recalled in Table IV.

B. Viscosity, self-diffusion and rotational correlation time of D_2O

For D_2O , we carefully collected all literature data that we could find and chose the most accurate values at each available temperature. We checked that at common temperatures, the selected data were in good agreement with each other.

The uncertainties given in the sources were considered as $1 - \sigma$ uncertainties (confidence interval 68%), unless otherwise stated in the article. Most authors provide uncertainties without stating whether the temperature uncertainty was propagated in the uncertainty on η , D_s or τ_θ . It is obviously not the case in Millero [24], Gonçalves [47], Matubayasi [60] and Hardy [57] since propagating the temperature uncertainty results in an uncertainty on η , D_s or τ_θ greater than the uncertainty provided in their papers. As a consequence, fitting their data by a Speedy-Angell law (eq. 6) and propagating the temperature uncertainty, we obtained the accuracies indicated in the tables. For other papers, the uncertainty on the temperature is compatible with the uncertainty

TABLE III. Selected previous datasets for the viscosity of H₂O at or near atmospheric pressure

First author and reference	Year	Accuracy (%)	Temperature range (K)	Number of data
Hallet [12]	1963	1	250.15 - 264.15	15
Korosi [31]	1968	0.3	348.15 - 423.15	7
Eicher [25]	1971	0.3	264.87 - 273.15	5
Kestin [32]	1981	0.3	343.70 - 423.96	4
Collings [26]	1983	0.2	274.15 - 288.15, 303.15 - 343.15	10
Kestin [23]	1985	0.5	458.55 - 491.95	3
Berstad [27]	1988	0.05	293.15 - 298.15	6
Dehaoui [9]	2015	2.9	239.15	1

TABLE IV. Best-fit parameters for a Speedy-Angell law (eq. 6). The fit of D_s and τ_θ of light water is the same as previously published [9].

Data A	Temperature range (K)	Number of points N	A_0	T_s (K)	γ	Reduced $\chi_{2,r} = \chi_2/(N - 3)$
η , H ₂ O	239.15-348.15	49	$137.4 \pm 0.3 \mu\text{Pa}\cdot\text{s}$	225.99 ± 0.14	1.636 ± 0.004	1.31
D_s , H ₂ O	237.8-498.2	36	$16077 \pm 78 \mu\text{m}^2/\text{s}$	213.96 ± 0.35	-2.0801 ± 0.0086	1.62
τ_θ , H ₂ O	236.18-451.63	51	$217.89 \pm 0.90 \text{ fs}$	223.05 ± 0.14	1.8760 ± 0.0065	0.61
η , D ₂ O	243.7-329.65	70	$140.53 \pm 0.07 \mu\text{Pa}\cdot\text{s}$	233.52 ± 0.12	1.599 ± 0.003	0.76
D_s , D ₂ O	244.2-373.15	28	$15720 \pm 140 \mu\text{m}^2/\text{s}$	220.1 ± 1.1	-2.06 ± 0.03	1.30
τ_θ , D ₂ O	239.0-473.15	47	$238.3 \pm 1.5 \text{ fs}$	230.79 ± 0.13	1.811 ± 0.007	0.77

on η , D_s or τ_θ and we decided to keep the provided uncertainty.

Due to the scant and often confusing information provided by the authors about their uncertainties, some differences exist between our tables V and VII and the ones provided by Assael [61] and Suárez-Iglesias [62].

1. Viscosity of D₂O

The existing sources of viscosity data for D₂O are gathered in Table V. Following Matsunaga [63], we discarded the data of Heiks [39]. Following Kestin [23], we discarded the data provided in 1968 by Agaev and Yusibova [41].

The most accurate sources we decided to use are gathered in Table VI. Note that we recalculated the data of Hardy, Millero, Kestin and Gonçalves using the current reference value for viscosity of pure light water at 293.15 K, $\eta(T_0) = 1.0016 \text{ mPa}\cdot\text{s}$ [22]. We chose to discard Jones' data point since it disagrees with Millero's data point at the same temperature, while Millero agrees with all the other authors at any temperature. We decided to consider only the data up to $T = 500 \text{ K}$. At that temperature, the vapor pressure is less than 30 bars, and dynamic properties of heavy water are nearly constant in that pressure range.

2. Self-diffusion of D₂O

The existing sources of self-diffusion data for D₂O are gathered in Table VII. The data of Longworth [49] were later reanalyzed by Mills [52], and we used the latter set of data.

Following Yoshida [59] and Suárez-Iglesias [62], we discarded the data published by Yoshida in 2005 [58]. Care must be taken about the data of Yoshida [59], that were measured under vapor pressure, because this reaches up to 167 bar at the highest temperature.

The data scatter of Price *et al.* [10] is not compatible with the uncertainties they provide, as already stated about their data on H₂O [9]. From the data scatter around a Speedy-Angell law fit, we estimate the actual uncertainty to 5%.

DeFries [46] does not provide any uncertainty in their article. We chose to apply the value provided by Wilbur [44], since they come from the same group, on the same equipment, at a one year interval.

The data of Woolf [53] and Weingärtner [54] were deduced from their measurements of the diffusion coefficient of DTO in D₂O in the same way as Mills [52] deduced the self-diffusion of H₂O and D₂O from the diffusion of isotopes [49, 52]. The results are reproduced in the table IX.

The most accurate sources we decided to use are gathered in Table XI.

The ratios $D_{s,\text{H}_2\text{O}}/D_{s,\text{D}_2\text{O}}$ of Hardy [57] were graphically read on their figure 2 and $D_{s,\text{D}_2\text{O}}$ was deduced using the value of $D_{s,\text{H}_2\text{O}}$ calculated following Eq. 6 with

TABLE V. Previous data sets for the viscosity of D₂O at or near atmospheric pressure.

First author and reference	year	Accuracy	Temperature range (K)	Number of data
Lewis [33]	1933	0.5%	278.15 to 308.15	7
Taylor [34]	1934	n.p.	293.15	1
Baker [35]	1935	0.1%	298.15	1
Jones [36]	1936	0.01%	298.15	1
Lemonde [37]	1941	n.p.	278.15 to 290.15	13
Hardy [38]	1949	0.1%	278.15 to 398.15	11
Heiks [39]	1954	3.10^{-6} Pa.s	303.15 to 523.15	12
Harlow [40]	1967	1%	283 to 373	7
Agaev [41]	1968	0.5%	277.15 to 348.15	10
Selecki [42]	1970	0.8%	298.15 to 363.15	6
Millero [24]	1971	3 to 8.10^{-7} Pa.s	278.15 to 343.15	28
Kellomäki [43]	1975	0.1%	283.15 to 308.15	6
Wilbur [44]	1976	2%	283 to 363	4
Jonas [45]	1976	2%	283 to 363	3
DeFries [46]	1977	2%	278 to 283	2
Gonçalves [47]	1979	0.02 to 0.06%	293.15 to 333.15	6
Agayev [29]	1980	0.5 to 1.2%	277.01 to 369.05	12
Kestin [23]	1985	0.5%	298.25 to 493.05	12
Agayev [30]	1989	0.6%	276.97	1
Harris [48]	2004	1%	278.15 to 298.15	9

TABLE VI. Selected previous data sets for the viscosity of D₂O at or near atmospheric pressure

First author and reference	year	Accuracy (%)	Temperature range (K)	Number of data
Hardy [38]	1949	0.1	353.15 to 398.15	7
Selecki [42]	1970	0.8%	348.15	1
Millero [24]	1971	3 to 8.10^{-7} Pa.s	278.15 to 308.15, 318.15, 328.15, 338.15, 343.15	22
Gonçalves [47]	1979	0.03 to 0.05%	313.15 to 333.15	3
Agayev [29]	1980	0.5 to 1.2%	277.01 to 300.75 305.59 to 369.05	11
Kestin [23]	1985	0.5%	298.25 to 493.05	12
Agayev [30]	1989	0.6%	276.97	1

parameters given in Table IV. An uncertainty on the reading was added to those data.

The most accurate sources we decided to use are gathered in Table VIII.

3. Rotational correlation time of D₂O

The existing sources of rotational correlation time data for D₂O are gathered in Table X. Most of the authors provide values of the spin-lattice relaxation time T_1 . Qvist [11] provides the rotational correlation time $\tau_\theta = \frac{1}{\omega_Q^2 T_1}$, $\omega_Q = 1.02 \cdot 10^6 \text{s}^{-1}$ being the nuclear quadrupole frequency of deuterium. Hardy *et al.* [57] provide the ra-

tio between the apparent rotational diffusion coefficients $D_{\text{rot}} = 1/(6 \tau_\theta)$ of light and heavy water. We decided to convert all those data into the rotational correlation time τ_θ .

The data of Hindman [64] and Matubayasi [60] are measured on the liquid-vapor equilibrium line. We decided to keep all the data of Hindman since in that temperature range, the vapor pressure does not exceed 10 bars, while the rotational correlation time is nearly constant in that pressure range. For the same reasons as above, we used Matubayasi's data only up to 500 K.

Hindman [64] and Qvist [11] do not provide their raw data. We read the temperature where they measured the rotational correlation time τ_θ (Qvist) or the spin-

TABLE VII. Data sets for the self-diffusion coefficient of D₂O at or near atmospheric pressure.

First author and reference	year	Accuracy	Temperature range (<i>K</i>)	Number of data
Longsworth [49]	1960	0.1%	278.15-318.15	3
Devell [50]	1962	1%	298.15	1
Murday [51]	1970	7%	294.3-295.2	3
Mills [52]	1973	0.2%	278-318	3
Wilbur [44]	1976	10%	283-363	4
Woolf [53]	1976	2%	280.5-328.2	7
DeFries [46]	1977	n.p.	278-283	2
Weingärtner [54]	1984	0.4 to 0.6%	281-318	3
Prielmeier [55]	1988	6%	258.0-363.0	11
Price [56]	2000	5%	244.2-298.25	17
Hardy [57]	2001	1.4 to 1.9%	288-328	7
Yoshida ^a [58]	2005	0.5 to 3%	303-623	18
Yoshida ^a [59]	2008	1 to 10%	303-623	33

^a Pressure up to 167 bar.

TABLE VIII. Selected data sets for the self-diffusion coefficient of D₂O at or near atmospheric pressure.

First author and reference	year	Accuracy	Temperature range (<i>K</i>)	Number of data
Mills [52]	1973	0.2%	278-318	3
Woolf [53]	1976	2%	280.5, 313.2	3
Weingärtner [54]	1984	0.6%	281	1
Prielmeier [55]	1988	6%	332.5-363.0	2
Price [56]	2000	5%	244.2-276.40	13
Hardy [57]	2001	1.4 to 1.9%	288, 293, 303, 308, 328	5
Yoshida ^a [59]	2008	1 to 10%	373-623	26

^a Pressure up to 167 bar.

TABLE IX. Self-diffusion of D₂O deduced from the measurements of Woolf [53] and Weingärtner [54]. For each D_s value the right reference is given.

<i>T</i> (<i>K</i>)	280.5	280.5	281.2	288.2	288.2	298.2	298.2	313.2	318.2	328.2
$D_s \times 10^9 \text{ m}^2/\text{s}$	1.05 [53]	1.06 [53]	1.12 [54]	1.36 [53]	1.37 [53]	1.87 [53]	1.87 [54]	2.67 [53]	2.99 [54]	3.60 [53]

TABLE X. Data sets for the rotational correlation time τ_θ of D₂O at or near atmospheric pressure.

First author and reference	year	Accuracy (%)	Temperature range (<i>K</i>)	Number of data
Hindman [64]	1971	3	263 - 447	24
Hindman [65]	1973	3 to 10%	236.1 - 287.6	35
Jonas [45]	1976	3%	283 - 363	3
DeFries [46]	1977	3%	278 - 283	2
Lang [66]	1980	10%	239 - 283	15
Matubayasi [60]	2001	3 to 13%	303 - 613	8
Ropp [67]	2001	1%	275.7 - 310.5	8
Hardy [57]	2001	2 to 3%	278 - 358	17
Qvist [11]	2012	0.5 to 2%	241 - 307	21

TABLE XI. Selected data sets for the rotational correlation time τ_θ of D₂O at or near atmospheric pressure.

First author and reference	year	Accuracy	Temperature range (K)	Number of data
Hindman [64]	1971	3	367 - 447	11
Jonas [45]	1976	3%	363	1
Lang [66]	1980	10%	239	1
Matubayasi [60]	2001	5%	473	1
Ropp [67]	2001	1%	310.5	1
Hardy [57]	2001	2 to 3%	308 - 358	11
Qvist [11]	2012	0.5 to 2%	241 - 307	21

TABLE XII. Best-fit parameters for a VTF law (eq. 7)

Data	Temperature range (K)	Number of points N	A_0	B (K)	T_0 (K)	Reduced $\chi_{2,r} = \chi_2/(N-3)$
η , H ₂ O	239.15-348.15	49	$43.3 \pm 0.4 \mu\text{Pa}\cdot\text{s}$	394 ± 3	167.6 ± 0.4	18
η , D ₂ O	243.7-329.65	70	$46.1 \pm 0.3 \mu\text{Pa}\cdot\text{s}$	402.6 ± 1.6	171.1 ± 0.3	6.8
D_s , D ₂ O	244.2-373.15	28	$75000 \pm 5000 \mu\text{m}^2/\text{s}$	-510 ± 20	159 ± 3	1.53
τ_θ , D ₂ O	239.0-473.15	47	$87.5 \pm 1.5 \text{ fs}$	361 ± 3	184.9 ± 0.4	28

lattice relaxation time T_1 (Hindman) on their figures and computed the expected value from the fits they provide. Ropp's data [67] are directly read on their Fig. 3. A reading uncertainty was added. Hardy's data [57] are read as explained in Section IV B 2 to deduce the rotational correlation time of D₂O from the fit of the rotational correlation time of H₂O (Eq. 6 with parameters given in Table IV).

V. DISCUSSION

A. Classic fits

The viscosity of light and heavy water clearly departs from an Arrhenius behaviour, as shown in Figs. 9 and 10 (left panels), showing that both isotopes behave as fragile glassformers.

The viscosity of H₂O and D₂O and the diffusion coefficient and rotational correlation time of D₂O were fitted by the classic expressions: the Speedy-Angell power-law (Eq. 3 or Eq. 6), and the Vogel-Tamman-Fulcher (VTF) law:

$$A(T) = A_0 \exp\left(\frac{B}{T - T_0}\right). \quad (7)$$

The temperature ranges and best-fit parameters are given in Tables IV and XII. The fits of viscosity are presented in Figs. 9 and 10 (center and right panels).

As expected from previous results [9], the Speedy-Angell law best describes dynamic data of light and heavy water over a large temperature range. The rotational correlation time is even well described by a Speedy-Angell law up to 473.15 K, even if the data are taken on the saturation line at the highest temperatures. The fits of

D_s and τ_θ by a Speedy-Angell law are shown in Fig. 11 to 14.

B. Comparison with mode coupling theory

Mode coupling theory [68] predicts a power-law dependence of dynamic quantities, similar to the Speedy-Angell formula. However, in the case of mode coupling, T_s refers to the mode-coupling temperature, and should be the same for all three quantities (D_s , η , and τ_θ). This is not what is experimentally observed, neither for light nor for heavy water. Mode coupling theory also predicts the products $D_s\eta$ and η/τ_θ to be temperature independent. Indeed, $D_s\eta$ is constant over a small temperature range (≈ 260 to 300 K) for both isotopes, as can be seen in Figs. 15 and 16, but it is not the case of η/τ_θ . Moreover, $D_s\eta$ increases sharply at lower temperatures, in contradiction with the predictions of mode coupling theory. Mode coupling theory is usually expected to be valid close enough to the glass transition temperature, a condition not met here. Still, experiments on Zr₆₄Ni₃₆ show that mode-coupling could hold up to $2T_s$ [69]. This is not the case for water: mode coupling theory fails in describing the dynamic quantities of light and heavy water in the experimentally accessible temperature range.

C. Stokes-Einstein and Stokes-Einstein-Debye relations

Using the selected data for the viscosity η , self-diffusion D_s and rotational correlation time τ_θ of heavy water (Tables VI, VIII, XI), we plot as a function of temperature in Figs. 17 and 18 the SE ratio $D_s\eta/T$ (upper panels)

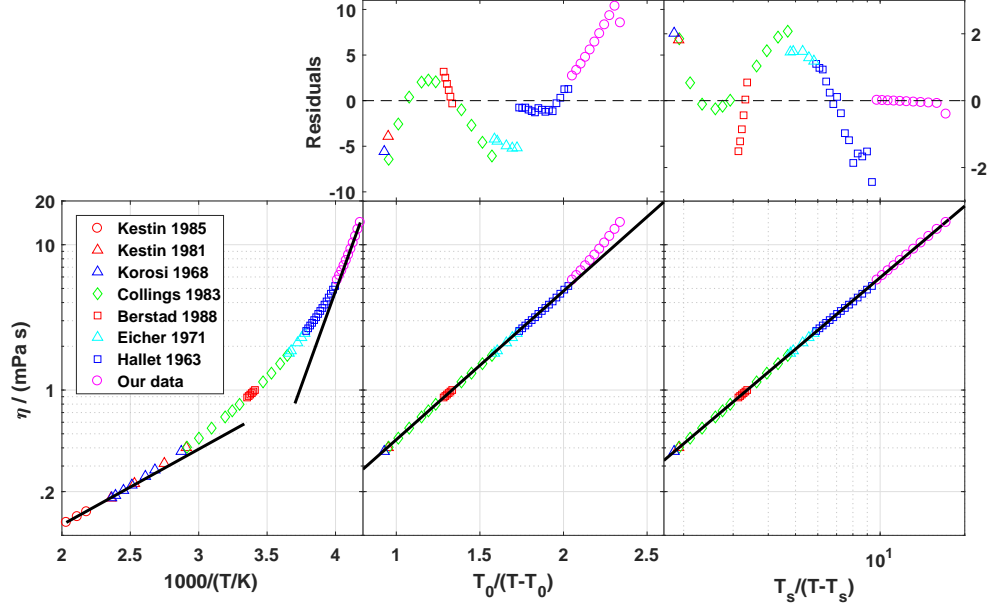


FIG. 9. Viscosity of light water in different representations. The three panels include the 8 datasets tabulated in Table III and our data (pink circles), together with a best-fit with various models (lines, see below). The lowest temperature pink circle is the one that was previously published in Ref. [9]. (Left) Arrhenius plot, showing an apparent activation energy increasing from 1200 to 6000 K upon cooling (solid lines). (Center) VTF representation, with best-fit parameters in Table XII). (Right) Speedy-Angell representation, with best-fit parameters in Table IV). (Top) The reduced residuals $(\eta_{\text{exp}} - \eta_{\text{fit}})/\sigma_{\text{exp}}$, where η_{exp} and η_{fit} are the experimental and fitted viscosity, respectively, and σ_{exp} is the experimental uncertainty (1 SD). Note the different vertical scale in the top right panel.

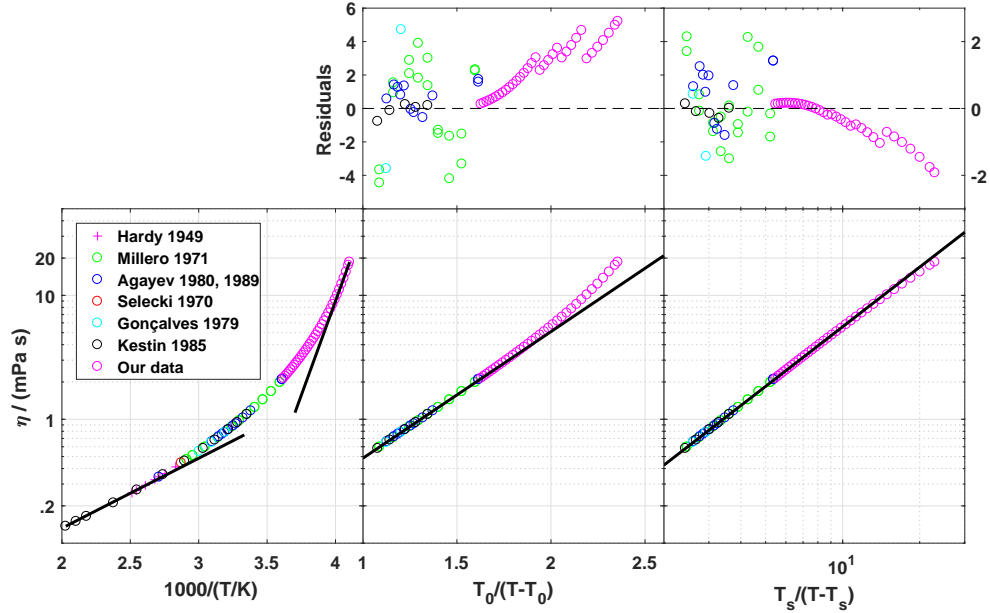


FIG. 10. Viscosity of heavy water in different representations. The three panels include the 7 datasets tabulated in Table VI and our data (pink circles), together with a best-fit with various models (lines, see below). (Left) Arrhenius plot, showing an apparent activation energy increasing from 1300 to 7000 K upon cooling (solid lines). (Center) VTF representation, with best-fit parameters in Table XII). (Right) Speedy-Angell representation, with best-fit parameters in Table IV). (Top) The reduced residuals $(\eta_{\text{exp}} - \eta_{\text{fit}})/\sigma_{\text{exp}}$, where η_{exp} and η_{fit} are the experimental and fitted viscosity, respectively, and σ_{exp} is the experimental uncertainty (1 SD). Note the different vertical scale in the top right panel.

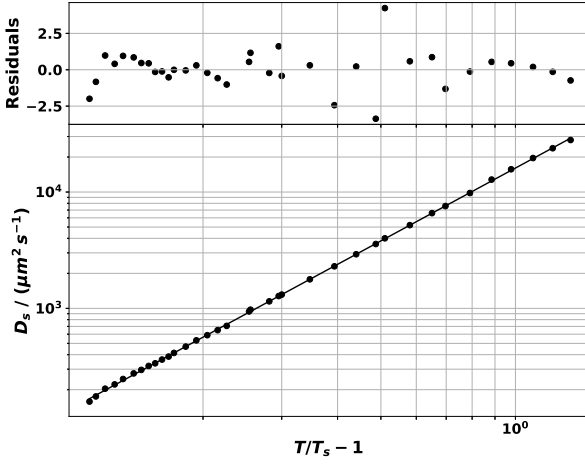


FIG. 11. Fit of the self-diffusion coefficient of light water by a Speedy-Angell law, with parameters given in Table IV.

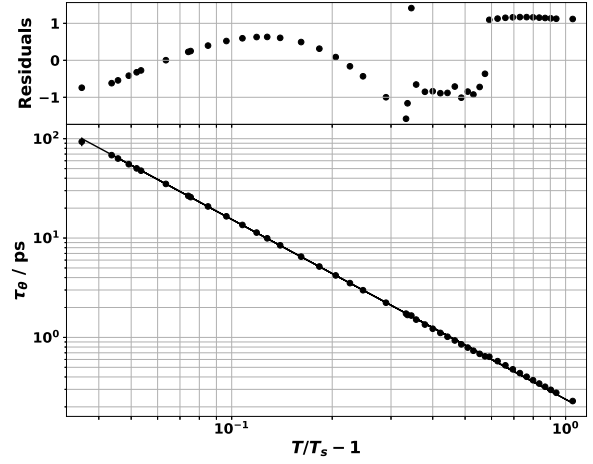


FIG. 14. Fit of the rotational correlation time of heavy water by a Speedy-Angell law, with parameters given in Table IV.

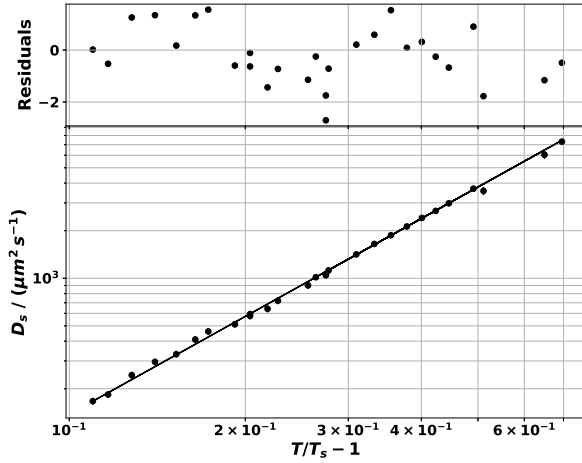


FIG. 12. Fit of the self-diffusion coefficient of heavy water by a Speedy-Angell law, with parameters given in Table IV.

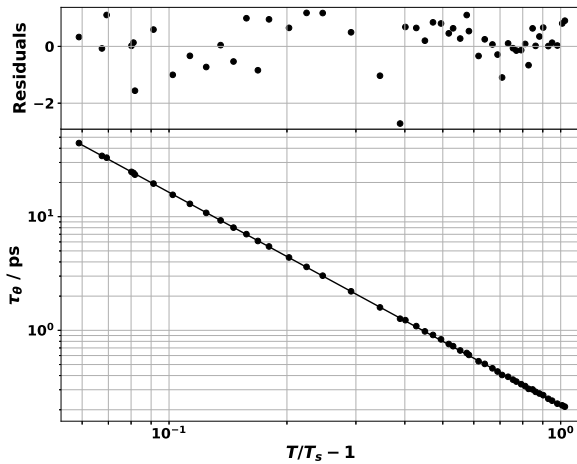


FIG. 13. Fit of the rotational correlation time of light water by a Speedy-Angell law, with parameters given in Table IV.

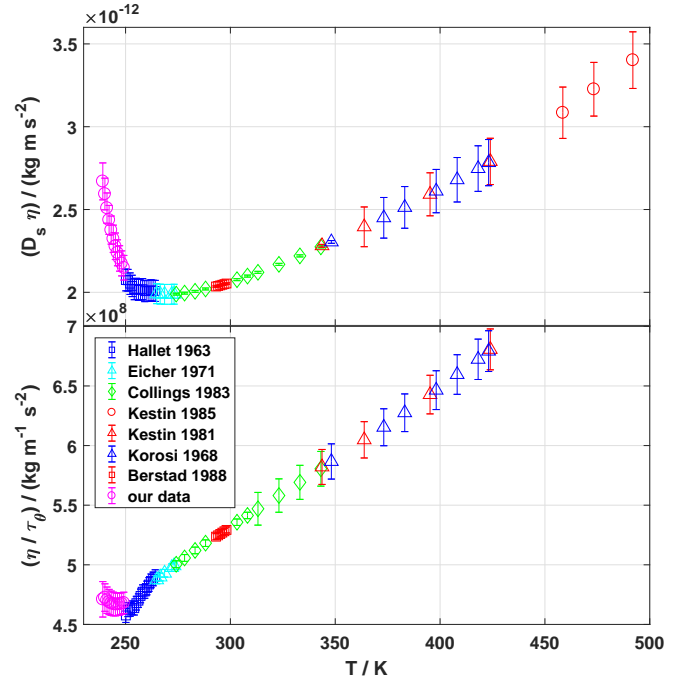


FIG. 15. Test of the predictions of the mode coupling theory on the dynamic quantities of light water: $D_s \eta$ (top) and η / τ_θ (bottom) should be constant according to the mode coupling theory.

and the SED ratio $\eta / (T \tau_\theta)$ (lower panels). In all panels the data are normalized by the value at 343.15 K. To generate all graphs presented in this section, we used the data points for η provided by the different authors, together with values of D_s and τ_θ computed at the same temperatures by a fitting function. For τ_θ , we use the Speedy-Angell fit with parameters given in Table IV. For D_s , as the Speedy-Angell fit fails at very high temperature, we use from 244 to 623 K the following function:

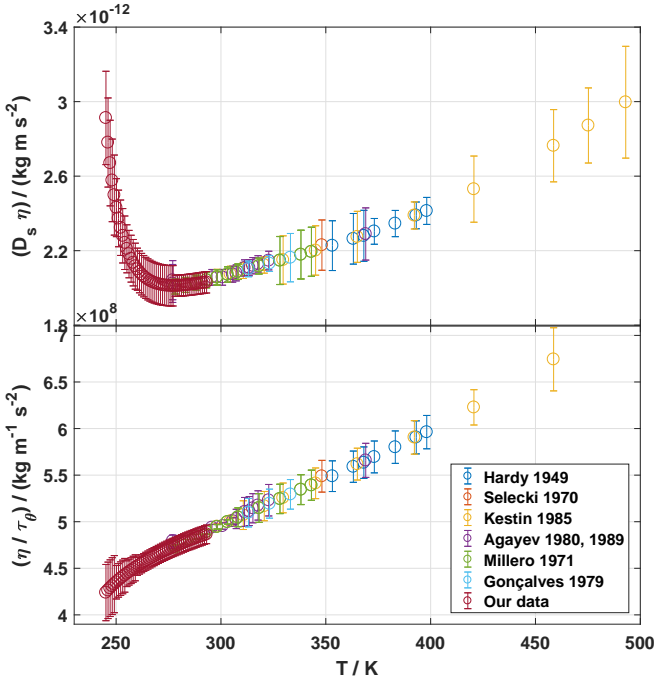


FIG. 16. Test of the predictions of the mode coupling theory on the dynamic quantities of heavy water: $D_s \eta$ (top) and η / τ_θ (bottom) should be constant according to the mode coupling theory.

TABLE XIII. Best-fit parameters for the function $\ln[D_s / (\text{m s}^{-2})] = \sum_{i=0}^5 A_i (\ln(T/K))^i$ from 244 to 623 K. $\chi_2 = 2.23$

i	A_i
0	$-1.655461201959378 \cdot 10^5$
1	$1.365289265726531 \cdot 10^5$
2	$-4.506424270204171 \cdot 10^4$
3	$7.439738201650022 \cdot 10^3$
4	$-6.142825158988378 \cdot 10^2$
5	20.292383150993103

$\ln[D_s / (\text{m s}^{-2})] = \sum_{i=0}^5 A_i (\ln(T/K))^i$, with best-fit parameters A_i 's given in Table XIII.

The results are quite similar in light and heavy water: SE and SED relations both hold at high temperature, but are increasingly violated as temperature decreases. The SE violation reaches 70% to 90% at the lowest temperature, with an increasing trend as the temperature decreases, while the SED violation only reaches 15% to 20%. Because the failure of SE and SED is progressive, it is not possible to precisely define a temperature at which the violation starts. Still, we can note that the degree of violation becomes significant around the triple points (273.16 K for H_2O and 276.969 K for D_2O), where all ratios reach around 1.1. In usual fragile glassformers, SE violation starts around $1.2 T_g$ [7], where T_g is the glass transition temperature. For water, T_g is reported to be

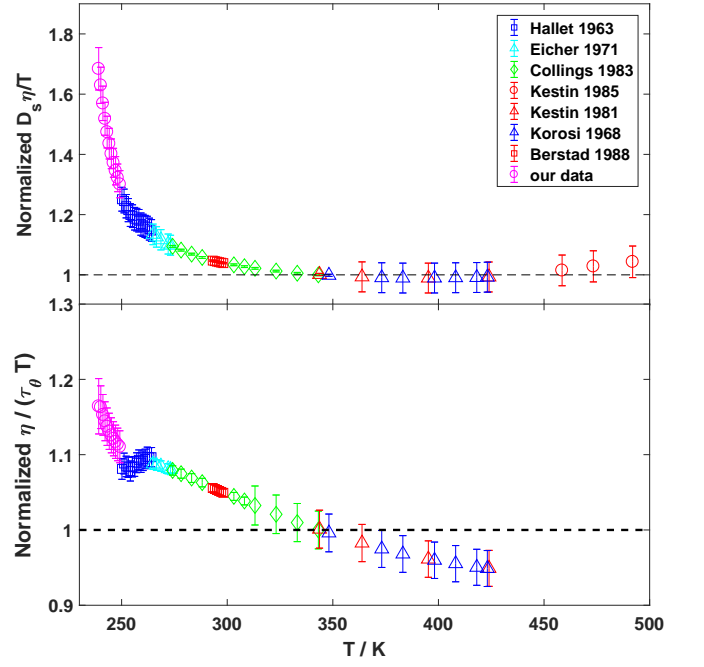


FIG. 17. Stokes-Einstein (top) and Stokes-Einstein-Debye (bottom) ratios as a function of temperature in light water.

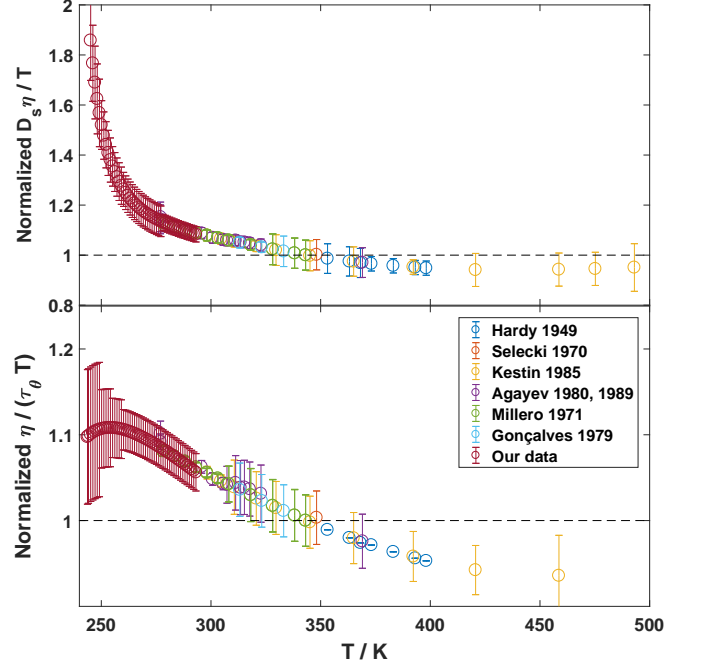


FIG. 18. Stokes-Einstein (top) and Stokes-Einstein-Debye (bottom) ratios as a function of temperature in heavy water.

131.8 and 135.6 K for H_2O and D_2O , respectively [70]. Therefore, SE violation already starts at anomalously high temperatures, above $2T_g$. It is important to note that this violation of the SE relation applies to the self-diffusion of water molecules, not to the Brownian diffusion of colloids that we used to deduce the viscosity of

the liquids (Eq. 1). Indeed, the sphere diameter we use (350 nm) is sufficiently large for hydrodynamic laws to hold.

We refer the reader to Ref. [71] for a discussion of the possible origin of the SE violation in water. In particular, it is shown there that the SE ratio for D₂O are equal to those for H₂O, shifted by +7 K in temperature. This suggests that the decoupling in both isotopes, albeit starting at different temperatures, may have a common origin, possibly related to the putative liquid-liquid transition in supercooled water [72].

The SE ratio in light water is in good agreement with the results from molecular dynamic simulations of the viscosity and the self-diffusion of light water at ambient pressure using the TIP4P/2005 water model [73, 74] and the TIP4P/2005f model [75]. In the latter study, the authors emphasize that the viscosity and the α -relaxation time are strongly coupled above 309 K but get uncoupled below that temperature. When investigating the SE and SED relations below that temperature, the shear-viscosity needs to be computed instead of the α -relaxation time as was frequently done before [76, 77].

The α -relaxation time has already been determined experimentally twice using the Optical Kerr Effect [78, 79]. In both studies it is found to be well described by a Speedy-Angell law with different fit parameters: in 2004 the authors determined $T_s = 221 \pm 5$ K and $\gamma = 2.2 \pm 0.3$. In 2013 they found $T_s = 227$ K and $\gamma = 1.7$ on a larger temperature range without providing their uncertainty. The precision on those experimental values is too low to allow concluding experimentally about the decoupling between the viscosity and the α -relaxation time.

Turning to the SED relation, the violation remains moderate down to 250 K, which is in line with simulations using the TIP4P/2005 water model [80]; see however Section I of the Supplemental Material for a more detailed discussion of SED relation in water.

D. Apparent hydrodynamic radius

The SE ratios displayed in Figs. 17 and 18 are normalized. This hides quantitative information about the effective hydrodynamic radius R_h of a water molecule, which can be defined by analogy with the Stokes-Einstein equation for a Brownian sphere, Eq. 1:

$$R_h = \frac{k_B T}{C \pi \eta D_s}, \quad (8)$$

C being a coefficient varying from 4 to 6 when the condition at the surface of the sphere changes from a full-slip to a no-slip condition, respectively. Choosing $C = 4$ yields R_h displayed in Fig. 19.

The definition of R_h with Eq. 8 is meaningful only when the SE relation holds; therefore, we plot only values above the triple point. Both isotopes have close values of $R_h \simeq 0.17$ nm. The 10% difference at the highest temperatures is not significant, as there is some uncertainty

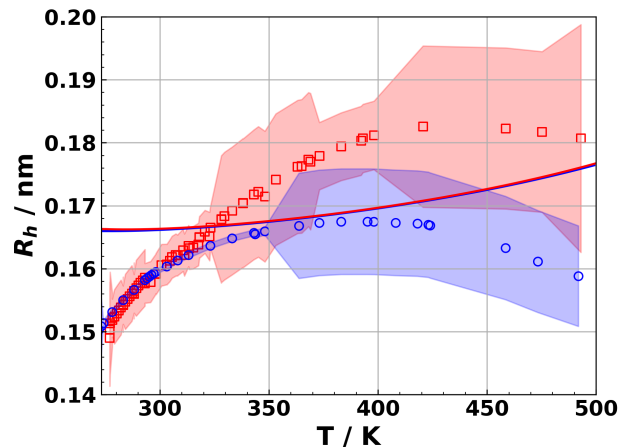


FIG. 19. Hydrodynamic radius R_h as a function of temperature calculated from Eq. 8 for H₂O (blue circles) and D₂O (red squares); the colored areas indicate the $1-\sigma$ uncertainty. The solid curves show R_{rcp} from Eq. 9 for H₂O (blue) and D₂O (red).

in the diffusion coefficient values at high temperatures, with up to 10% discrepancy between authors for H₂O at 373 K [59, 81]. It is interesting to compare R_h to a typical molecular size. We define it from the molar volumes V_{mol} of H₂O [82] and D₂O [83], as the radius R_{rcp} of hard spheres whose random close packing leads to the same molar volume:

$$R_{\text{rcp}} = \left(\frac{3}{4\pi} \frac{\phi V_{\text{mol}}}{\mathcal{N}_A} \right)^{1/3}. \quad (9)$$

Here $\phi = 0.64$ is the compaction for random-close packing, and \mathcal{N}_A the Avogadro constant. Figure 19 shows that R_{rcp} and R_h are in good agreement for both isotopes above 300 K. This is a rather surprising result, as the continuous medium approximation behind the SE relation would be expected to fail at the molecular level.

E. Fractional Stokes-Einstein and Stokes-Einstein-Debye relations

To account for the deviations from the SE relation, the so-called fractional SE relations have been introduced :

$$\frac{D_s}{T} \propto \eta^{-t}, \quad (10)$$

or alternatively:

$$D_s \propto \left(\frac{\eta}{T} \right)^{-\zeta}. \quad (11)$$

Such relations perform well for a variety of liquids, as well as for simulation data on the Lennard-Jones fluid (see Ref. [84] for a review). To justify the fractional SE relations, some theoretical arguments have been given [84].

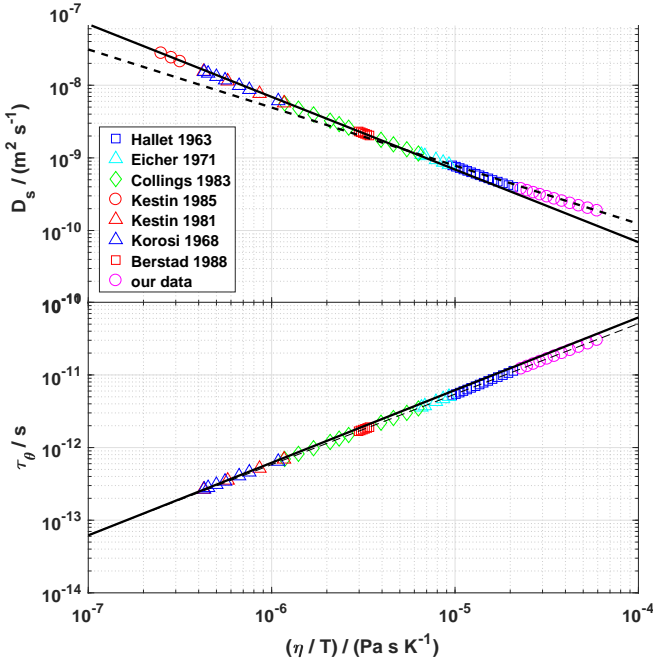


FIG. 20. Fractional Stokes-Einstein (top) and Stokes-Einstein-Debye (bottom) ratios as a function of viscosity in light water. Straight lines: Stokes-Einstein and Stokes-Einstein-Debye relations. Dashed line: $D_s \propto (\eta/T)^{-0.8}$ (top); $\tau_\theta \propto (\eta/T)^{0.9704}$ (bottom).

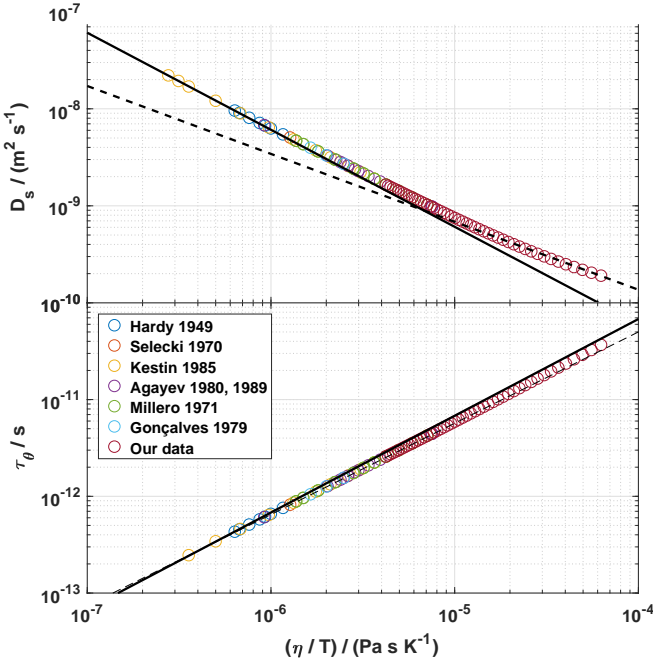


FIG. 21. Fractional Stokes-Einstein (top) and Stokes-Einstein-Debye (bottom) ratios as a function of viscosity in heavy water. Straight lines: Stokes-Einstein and Stokes-Einstein-Debye relations. Dashed line: $D_s \propto (\eta/T)^{-0.7}$ (top); $\tau_\theta \propto (\eta/T)^{0.9567}$ (bottom).

An obstruction model [85], which assumes diffusion amid obstructions representing dynamic heterogeneities, predicts Eq. 11 with $\zeta = 3/5$. An entropic barrier hopping theory of glassy hard sphere colloidal suspensions [86] finds fractional SE behavior with ζ ranging from 0.73 to 0.90, depending on the density fluctuation correlation length. For the rotational correlation time τ_θ , a fractional SED relation similar to Eq. 11,

$$\tau_\theta \propto \left(\frac{\eta}{T}\right)^\zeta, \quad (12)$$

has been first used for a tracer in ortho-terphenyl [87].

We test Eqs. 11 and 12 in Figs. 20 and 21 for light and heavy water, respectively. At high temperatures, the SE relation holds ($\zeta = 1$). At low temperatures, ζ switches from 1 to 0.8 (resp. 0.7) in H_2O (resp. D_2O). The fractional Stokes-Einstein-Debye relation Eq. 12 holds with a constant exponent 0.9704 in H_2O and 0.9567 in D_2O on the whole temperature range for both isotopes. The experimental behavior is similar to that found in simulations. In a study of the ST2 water model [76], the α -relaxation time τ_α was used as a proxy for viscosity. D_s and τ_θ were analyzed with the analogs of Eqs. 11 and 12, respectively. Upon cooling, ζ for D_s switches from 1 to 0.7 – 0.8, while $\zeta = 0.9$ represents well τ_θ at low temperature. In Ref. [80], η was directly simulated instead of τ_α and suggests ζ switching from 1 to $\simeq 0.7$ for D_s and $\zeta \gtrsim 0.8$ for τ_θ .

VI. CONCLUSION

We have obtained new measurements of the viscosity of H_2O with a better accuracy than in our previous work [9], and the first reliable measurements of the viscosity of deeply supercooled D_2O . It appears that previous measurements on heavy water by Osipov [13] are biased, possibly due to an electroosmosis effect, as we already suggested in the case of light water [9]. The temperature dependence of dynamic properties of D_2O (viscosity, self-diffusion, and rotational correlation time) obeys a Speedy-Angell power-law, like in the case of H_2O . The violation of the SE relation is similar in both isotopes, reaching at the lowest temperature above 70% and 80% for light and heavy water, respectively. The SED relation also shows a similar behavior in H_2O and D_2O , with only a mild violation less than 20%. Even if those two features are characteristic of fragile glassformers close to the glass transition temperature, as predicted by mode coupling theory, both isotopes significantly differ from other glassformers. The main difference is the unusually high temperature at which decoupling between dynamic quantities occurs, more than twice the glass transition temperature, while this decoupling occurs around $1.2T_g$ in usual glassformers. Deviations from the predictions of the mode coupling theory are also observed.

The decoupling between dynamic quantities in molecular glassformers is often attributed to dynamic hetero-

geneities [88]. Our results suggest that dynamic heterogeneities exist in both light and heavy water far above the glass transition temperature. Many molecular dynamic simulations find such heterogeneities and SE violation on light water [73, 76, 77, 89–92]. Those features are found in simulations where a liquid-liquid transition occurs in deeply metastable water [73, 76, 77, 89], as well as in simulations without such a transition [92]. Phenomenological two-state models [93], which treats water as a non-ideal mixture of inter-converting species, whose fraction depends on temperature and pressure, successfully reproduce thermodynamic and dynamic data of real [94–97] and simulated [73, 98] supercooled water. They are compatible with the existence of a liquid-liquid transition, but this is not necessary [99]. The vicinity of a critical point terminating a liquid-liquid transition, or the molec-

ular fluctuations between two different local structures, could induce dynamic heterogeneities in bulk light and heavy water, and provide a rationale to explain our observations.

ACKNOWLEDGMENTS

We acknowledge support from Agence Nationale de la Recherche, grant number ANR-19-CE30-0035-01.

Appendix: Smoothed values of the viscosity

-
- [1] C. A. Angell, Formation of Glasses from Liquids and Biopolymers, *Science* **267**, 1924 (1995).
- [2] K. Ito, C. T. Moynihan, and C. A. Angell, Thermodynamic determination of fragility in liquids and a fragile-to-strong liquid transition in water, *Nature* **398**, 492 (1999).
- [3] C. Goy, M. A. C. Potenza, S. Dederá, M. Tomut, E. Guillerm, A. Kalinin, K.-O. Voss, A. Schottelius, N. Petridis, A. Prosvetov, G. Tejada, J. M. Fernández, C. Trautmann, F. Caupin, U. Glasmacher, and R. E. Grisenti, Shrinking of Rapidly Evaporating Water Microdroplets Reveals their Extreme Supercooling, *Phys. Rev. Lett.* **120**, 015501 (2018).
- [4] See Supplemental Material [url] which include Refs. [5, 6], a discussion of molecular reorientation in water, and raw data tables.
- [5] P. J. W. Debye, *Polar Molecules* (Dover Publications, New York, 1929).
- [6] D. Laage and J. T. Hynes, A Molecular Jump Mechanism of Water Reorientation, *Science* **311**, 832 (2006).
- [7] I. Chang and H. Sillescu, Heterogeneity at the glass transition: Translational and rotational self-diffusion, *J. Phys. Chem. B* **101**, 8794 (1997).
- [8] M. T. Cicerone and M. D. Ediger, Photobleaching technique for measuring ultraslow reorientation near and below the glass transition: Tetracene in o-terphenyl, *J. Phys. Chem.* **97**, 10489 (1993).
- [9] A. Dehaoui, B. Issenmann, and F. Caupin, Viscosity of deeply supercooled water and its coupling to molecular diffusion, *Proc. Natl. Acad. Sci.* **112**, 12020 (2015).
- [10] W. S. Price, H. Ide, and Y. Arata, Self-diffusion of supercooled water to 238K using PGSE NMR diffusion measurements, *J. Phys. Chem. A* **103**, 448 (1999).
- [11] J. Qvist, C. Mattea, E. P. Sunde, and B. Halle, Rotational dynamics in supercooled water from nuclear spin relaxation and molecular simulations, *J. Chem. Phys.* **136**, 204505 (2012).
- [12] J. Hallett, The temperature dependence of the viscosity of supercooled water, *Proc. Phys. Soc.* **82**, 1046 (1963).
- [13] Y. A. Osipov, B. V. Zheleznyi, and N. F. Bondarenko, The shear viscosity of water supercooled to -35°C, *Russ. J. Phys. Chem.* **51**, 748 (1977).
- [14] M. Ceriotti, W. Fang, P. G. Kusalik, R. H. McKenzie, A. Michaelides, M. A. Morales, and T. E. Markland, Nuclear Quantum Effects in Water and Aqueous Systems: Experiment, Theory, and Current Challenges, *Chem. Rev.* **116**, 7529 (2016).
- [15] T. Maitra, C. Antonini, M. K. Tiwari, A. Mularczyk, Z. Imeri, P. Schoch, and D. Poulikakos, Supercooled Water Drops Impacting Superhydrophobic Textures, *Langmuir* **30**, 10855 (2014).
- [16] M. Schremb, I. V. Roisman, and C. Tropea, Normal impact of supercooled water drops onto a smooth ice surface: Experiments and modelling, *J. Fluid Mech.* **835**, 1087 (2018).
- [17] B. Ding, H. Wang, X. Zhu, R. Chen, and Q. Liao, How supercooled superhydrophobic surfaces affect dynamic behaviors of impacting water droplets?, *International Journal of Heat and Mass Transfer* **124**, 1025 (2018).
- [18] R. Cerbino and V. Trappe, Differential Dynamic Microscopy: Probing Wave Vector Dependent Dynamics with a Microscope, *Phys. Rev. Lett.* **100**, 188102 (2008).
- [19] F. Giavazzi, D. Brogioli, V. Trappe, T. Bellini, and R. Cerbino, Scattering information obtained by optical microscopy: Differential dynamic microscopy and beyond, *Phys. Rev. E* **80**, 031403 (2009).
- [20] Section 3: Physical Constants of Organic Compounds, in *CRC Handbook of Chemistry and Physics, 95th Ed* (CRC Press, 2014) Haynes, W. M. ed., pp. 1–553.
- [21] V. K. la Mer and W. N. Baker, The Freezing Point of Mixtures of H₂O and D₂O. The Latent Heat of Fusion of D₂O, *J. Am. Chem. Soc.* **56**, 2641 (1934).
- [22] M. L. Huber, R. A. Perkins, A. Laesecke, D. G. Friend, J. V. Sengers, M. J. Assael, I. N. Metaxa, E. Vogel, R. Mareš, and K. Miyagawa, New international formulation for the viscosity of H₂O, *J. Phys. Chem. Ref. Data* **38**, 101 (2009).
- [23] J. Kestin, N. Imaishi, S. H. Nott, J. C. Nieuwoudt, and J. V. Sengers, Viscosity of light and heavy water and their mixtures, *Physica A* **134**, 38 (1985).
- [24] F. J. Millero, R. Dexter, and E. Hoff, Density and viscosity of deuterium oxide solutions from 5-70 deg., *J. Chem. Eng. Data* **16**, 85 (1971).

- [25] L. D. Eicher and B. J. Zwolinski, High-precision viscosity of supercooled water and analysis of the extended range temperature coefficient, *J. Phys. Chem.* **75**, 2016 (1971).
- [26] A. F. Collings and N. Bajenov, A high precision capillary viscometer and further relative results for the viscosity of water, *Metrologia* **19**, 61 (1983).
- [27] D. Berstad, B. Knapstad, M. Lamvik, P. Skjølvik, K. Tørklep, and H. Øye, Accurate measurements of the viscosity of water in the temperature range 19.5–25.5°C, *Physica A: Statistical Mechanics and its Applications* **151**, 248 (1988).
- [28] J. Kestin, M. Sokolov, and W. A. Wakeham, Viscosity of liquid water in the range -8°C to 150°C, *J. Phys. Chem. Ref. Data* **7**, 941 (1978).
- [29] N. Agayev, Experimental investigation of the viscosity of ordinary and heavy water and steam in the temperature range from -10 to 375°C and at pressures from 0.1 to 200 MPa, in *Proc. 9th Int. Conf. Properties of Steam, Munich 1979* (Pergamon, Oxford, 1980) pp. 148–154.
- [30] N. Agayev, Heavy-Water viscosity under high pressures near freezing line, in *Proc. 11th Int. Conf. Properties of Water and Steam 1989, Prague* (1990) pp. 148–154.
- [31] A. Korosi and B. M. Fabuss, Viscosity of liquid water from 25 to 150.degree. measurements in pressurized glass capillary viscometer, *Anal. Chem.* **40**, 157 (1968).
- [32] J. Kestin and J. R. Shankland, The Free Disk as an Absolute Viscometer and the Viscosity of Water in the Range 25–150 °C, *J. Non-Equilib. Thermodyn.* **6**, 10.1515/jnet.1981.6.4.241 (1981).
- [33] G. N. Lewis and R. T. Macdonald, THE VISCOSITY OF H₂H₂O, *J. Am. Chem. Soc.* **55**, 4730 (1933).
- [34] H. S. Taylor and P. W. Selwood, SOME PROPERTIES OF HEAVY WATER, *J. Am. Chem. Soc.* **56**, 998 (1934).
- [35] W. N. Baker and V. K. La Mer, The Conductance of Potassium Chloride and of Hydrochloric-Deuteriochloric Acid H₂O—D₂O Mixtures. The Viscosity of H₂O—D₂O, *J. Chem. Phys.* **3**, 406 (1935).
- [36] G. Jones and H. J. Fornwalt, The Viscosity of Deuterium Oxide and Its Mixtures with Water at 25°C, *J. Chem. Phys.* **4**, 30 (1936).
- [37] H. Lemonde, Sur la viscosité de l'eau lourde, à différentes températures, *Comptes Rendus Académie Sci.* **212**, 81 (1941).
- [38] R. C. Hardy and R. L. Cottingham, Viscosity of deuterium oxide and water in the range 5 to 125 C, *J. RES. NATL. BUR. STAN.* **42**, 573 (1949).
- [39] J. R. Heiks, M. K. Barnett, L. V. Jones, and E. Orban, The Density, Surface Tension and Viscosity of Deuterium Oxide at Elevated Temperatures, *J. Phys. Chem.* **58**, 488 (1954).
- [40] A. Harlow, Further investigations into the effect of high pressure on the viscosity of liquids, (1967).
- [41] N. Agaev and A. Yusibova, Viscosity of ordinary water and heavy water at high pressures within 0-150 °C range, *Sov. Phys. Dokl.* **13**, 472 (1968).
- [42] A. Selecki, B. Tyminski, and A. G. Chmielewski, Viscosity of solutions of some electrolytes in heavy water, *J. Chem. Eng. Data* **15**, 127 (1970).
- [43] A. Kellomäki, Viscosities of {H₂O D₂O} mixtures at various temperatures, *Finn. Chem. Lett.* **2**, 51 (1975).
- [44] D. J. Wilbur, T. DeFries, and J. Jonas, Self-diffusion in compressed liquid heavy water, *J. Chem. Phys.* **65**, 1783 (1976).
- [45] J. Jonas, T. DeFries, and D. J. Wilbur, Molecular motions in compressed liquid water, *J. Chem. Phys.* **65**, 582 (1976).
- [46] T. DeFries and J. Jonas, Molecular motions in compressed liquid heavy water at low temperatures, *J. Chem. Phys.* **66**, 5393 (1977).
- [47] F. Gonçalves, The viscosity of {H₂O + D₂O} mixtures in the range 20 - 60°C, in *Proc. 9th Int. Conf. Properties of Steam, Munich 1979* (Pergamon, Oxford, 1980) j. straub and k. scheffler ed., pp. 354–361.
- [48] R. Harris and L. A. Woolf, Temperature and Volume Dependence of the Viscosity of Water and Heavy Water at Low Temperatures, *J. Chem. Eng. Data* **49**, 1064 (2004).
- [49] L. G. Longworth, The mutual diffusion of light and heavy water, *J. Phys. Chem.* **64**, 1914 (1960).
- [50] L. Devell, Measurements of the Self-diffusion of Water in Pure Water, {H₂O-D₂O} Mixtures and Solutions of Electrolytes, *Acta Chem. Scand.* **16**, 2177 (1962).
- [51] J. S. Murday and R. M. Cotts, Self-Diffusion in Liquids: H₂O, D₂O, and Na, *J. Chem. Phys.* **53**, 4724 (1970).
- [52] R. Mills, Self-diffusion in normal and heavy water in the range 1-45°, *J. Phys. Chem.* **77**, 685–688 (1973).
- [53] L. A. Woolf, Tracer diffusion of tritiated heavy water (D₂O) in heavy water (D₂O) under pressure, *J. Chem. Soc., Faraday Trans. 1* **72**, 1267 (1976).
- [54] H. Weingärtner, Diffusion in Liquid Mixtures of Light and Heavy Water, *Berichte Bunsenges. Für Phys. Chem.* **88**, 47 (1984).
- [55] F. X. Prielmeier, E. W. Lang, R. J. Speedy, and H.-D. Lüdemann, The pressure dependence of self diffusion in supercooled light and heavy water, *Berichte Bunsenges. Für Phys. Chem.* **92**, 1111 (1988).
- [56] W. S. Price, H. Ide, Y. Arata, and O. Söderman, Temperature dependence of the self-diffusion of supercooled heavy water to 244 K, *J. Phys. Chem. B* **104**, 5874 (2000).
- [57] E. H. Hardy, A. Zygar, M. D. Zeidler, M. Holz, and F. D. Sacher, Isotope effect on the translational and rotational motion in liquid water and ammonia, *The Journal of Chemical Physics* **114**, 3174 (2001).
- [58] K. Yoshida, C. Wakai, N. Matubayasi, and M. Nakahara, A new high-temperature multinuclear-magnetic-resonance probe and the self-diffusion of light and heavy water in sub- and supercritical conditions, *J. Chem. Phys.* **123**, 164506 (2005).
- [59] K. Yoshida, N. Matubayasi, and M. Nakahara, Self-diffusion coefficients for water and organic solvents at high temperatures along the coexistence curve, *The Journal of Chemical Physics* **129**, 214501 (2008).
- [60] N. Matubayasi, N. Nakao, and M. Nakahara, Structural study of supercritical water. III. Rotational dynamics, *J. Chem. Phys.* **114**, 4107 (2001).
- [61] M. J. Assael, S. A. Monogenidou, M. L. Huber, R. A. Perkins, and J. V. Sengers, New International Formulation for the Viscosity of Heavy Water, *Journal of Physical and Chemical Reference Data* **50**, 033102 (2021).
- [62] O. Suárez-Iglesias, I. Medina, M. d. I. Á. Sanz, C. Pizarro, and J. L. Bueno, Self-Diffusion in Molecular Fluids and Noble Gases: Available Data, *J. Chem. Eng. Data* **60**, 2757 (2015).
- [63] N. Matsunaga and A. Nagashima, Transport Properties of Liquid and Gaseous D₂O over

- a Wide Range of Temperature and Pressure, *J. Phys. Chem. Ref. Data* **12**, 933 (1983).
- [64] J. C. Hindman, A. J. Zielen, A. Svirnickas, and M. Wood, Relaxation Processes in Water. The Spin-Lattice Relaxation of the Deuteron in D₂O and Oxygen-17 in H₂¹⁷O, *J. Chem. Phys.* **54**, 621 (1971).
- [65] J. C. Hindman and A. Svirnickas, Relaxation processes in water. Spin-lattice relaxation of heavy water in supercooled water, *J. Phys. Chem.* **77**, 2487 (1973).
- [66] E. Lang and H.-D. Lüdemann, Pressure and Temperature Dependence of the Longitudinal Deuterium Relaxation Times in Supercooled Heavy Water to 300 MPa and 188 K, *Berichte der Bunsengesellschaft für physikalische Chemie* **84**, 462 (1980).
- [67] J. Ropp, C. Lawrence, T. C. Farrar, and J. L. Skinner, Rotational Motion in Liquid Water Is Anisotropic: A Nuclear Magnetic Resonance and Molecular Dynamics Simulation Study, *J. Am. Chem. Soc.* **123**, 8047 (2001).
- [68] W. Gotze and L. Sjogren, Relaxation processes in supercooled liquids, *Rep. Prog. Phys.* **55**, 241 (1992).
- [69] J. Brillo, A. I. Pommrich, and A. Meyer, Relation between Self-Diffusion and Viscosity in Dense Liquids: New Experimental Results from Electrostatic Levitation, *Phys. Rev. Lett.* **107**, 165902 (2011).
- [70] J. J. Shephard and C. G. Salzmann, Molecular Reorientation Dynamics Govern the Glass Transitions of the Amorphous Ices, *J. Phys. Chem. Lett.* **7**, 2281 (2016).
- [71] F. Caupin, P. Ragueneau, and B. Isenmann, Giant dynamic isotope effect in supercooled water, *ArXiv:2112.09010 Cond-Mat Physicsphysics* (2022), [arXiv:2112.09010 \[cond-mat, physics:physics\]](https://arxiv.org/abs/2112.09010).
- [72] P. Gallo, K. Amann-Winkel, C. A. Angell, M. A. Anisimov, F. Caupin, C. Chakravarty, E. Lascaris, T. Loerting, A. Z. Panagiotopoulos, J. Russo, J. A. Sellberg, H. E. Stanley, H. Tanaka, C. Vega, L. Xu, and L. G. M. Pettersson, Water: A Tale of Two Liquids, *Chem. Rev.* **116**, 7463 (2016).
- [73] P. Montero de Hijes, E. Sanz, L. Joly, C. Valeriani, and F. Caupin, Viscosity and self-diffusion of supercooled and stretched water from molecular dynamics simulations, *The Journal of Chemical Physics* **149**, 094503 (2018).
- [74] S. Dueby, V. Dubey, and S. Daschakraborty, Decoupling of Translational Diffusion from the Viscosity of Supercooled Water: Role of Translational Jump Diffusion, *J. Phys. Chem. B* **123**, 7178 (2019).
- [75] E. Guillaud, S. Merabia, D. de Ligny, and L. Joly, Decoupling of viscosity and relaxation processes in supercooled water: A molecular dynamics study with the TIP4P/2005f model, *Phys. Chem. Chem. Phys.* **19**, 2124 (2017).
- [76] S. Becker, P. Poole, and F. Starr, Fractional Stokes-Einstein and Debye-Stokes-Einstein relations in a network-forming liquid, *Phys. Rev. Lett.* **97**, 055901 (2006).
- [77] P. Kumar, S. V. Buldyrev, S. R. Becker, P. H. Poole, F. W. Starr, and H. E. Stanley, Relation between the Widom line and the breakdown of the Stokes-Einstein relation in supercooled water, *Proc. Natl. Acad. Sci. U.S.A.* **104**, 9575 (2007).
- [78] R. Torre, P. Bartolini, and R. Righini, Structural relaxation in supercooled water by time-resolved spectroscopy, *Nature* **428**, 296 (2004).
- [79] A. Taschin, P. Bartolini, R. Eramo, R. Righini, and R. Torre, Evidence of two distinct local structures of water from ambient to supercooled conditions, *Nat. Commun.* **4**, 2401 (2013).
- [80] T. Kawasaki and K. Kim, Spurious violation of the Stokes-Einstein-Debye relation in supercooled water, *Sci Rep* **9**, 8118 (2019).
- [81] K. Krynicki, C. D. Green, and D. W. Sawyer, Pressure and temperature dependence of self-diffusion in water, *Faraday Discuss. Chem. Soc.* **66**, 199 (1978).
- [82] W. Wagner and A. Pruss, International Equations for the Saturation Properties of Ordinary Water Substance. Revised According to the International Temperature Scale of 1990. Addendum to *J. Phys. Chem. Ref. Data* **16**, 893 (1987), *Journal of Physical and Chemical Reference Data* **22**, 783 (1993).
- [83] S. Herrig, M. Thol, A. H. Harvey, and E. W. Lemmon, A Reference Equation of State for Heavy Water, *Journal of Physical and Chemical Reference Data* **47**, 043102 (2018).
- [84] K. R. Harris, The fractional Stokes-Einstein equation: Application to Lennard-Jones, molecular, and ionic liquids, *J. Chem. Phys.* **131**, 054503 (2009).
- [85] J. Douglas and D. Leporini, Obstruction model of the fractional Stokes-Einstein relation in glass-forming liquids, *Journal of Non-Crystalline Solids* **235-237**, 137 (1998).
- [86] K. S. Schweizer and E. J. Saltzman, Activated Hopping, Barrier Fluctuations, and Heterogeneity in Glassy Suspensions and Liquids, *J. Phys. Chem. B* **108**, 19729 (2004).
- [87] L. Andreatti, A. D. Schino, M. Giordano, and D. Leporini, A study of the Debye - Stokes - Einstein law in supercooled fluids, *J. Phys.: Condens. Matter* **8**, 9605 (1996).
- [88] M. D. Ediger, Spatially heterogeneous dynamics in supercooled liquids, *Annu. Rev. Phys. Chem.* **51**, 99 (2000).
- [89] M. Mazza, N. Giovambattista, H. Stanley, and F. Starr, Connection of translational and rotational dynamical heterogeneities with the breakdown of the Stokes-Einstein and Stokes-Einstein-Debye relations in water, *Phys. Rev. E* **76**, 031203 (2007).
- [90] D. T. Limmer and D. Chandler, The putative liquid-liquid transition is a liquid-solid transition in atomistic models of water. II, *J. Chem. Phys.* **138**, 214504 (2013).
- [91] D. T. Limmer, *On the Fluctuations That Order and Frustrate Liquid* (University of California, Berkeley, 2013).
- [92] E. B. Moore and V. Molinero, Growing correlation length in supercooled water, *J. Chem. Phys.* **130**, 244505 (2009).
- [93] M. A. Anisimov, M. Duška, F. Caupin, L. E. Amrhein, A. Rosenbaum, and R. J. Sadus, Thermodynamics of Fluid Polyamorphism, *Phys. Rev. X* **8**, 011004 (2018).
- [94] V. Holten, J. V. Sengers, and M. A. Anisimov, Equation of State for Supercooled Water at Pressures up to 400 MPa, *J. Phys. Chem. Ref. Data* **43**, 043101 (2014).
- [95] L. P. Singh, B. Isenmann, and F. Caupin, Pressure dependence of viscosity in supercooled water and a unified approach for thermodynamic and dynamic anomalies of water, *Proc. Natl. Acad. Sci.* **114**, 4312 (2017).
- [96] F. Caupin and M. A. Anisimov, Thermodynamics of supercooled and stretched water: Unifying two-structure description and liquid-vapor spinodal, *J. Chem. Phys.* **151**, 034503 (2019).
- [97] M. Duška, Water above the spinodal, *J. Chem. Phys.* **152**, 174501 (2020).

- [98] J. W. Biddle, R. S. Singh, E. M. Sparano, F. Ricci, M. A. González, C. Valeriani, J. L. F. Abascal, P. G. Debenedetti, M. A. Anisimov, and F. Caupin, Two-structure thermodynamics for the TIP4P/2005 model of water covering supercooled and deeply stretched regions, *J. Chem. Phys.* **146**, 034502 (2017).
- [99] F. Caupin and M. A. Anisimov, Minimal microscopic model for liquid polyamorphism and water-like anomalies, [ArXiv210408117 Cond-Mat Physicsphysics](#) (2021), [arXiv:2104.08117 \[cond-mat, physics:physics\]](#).

TABLE XIV. Smoothed values of the viscosity of H₂O (resp. D₂O) as functions of the temperature: $\eta = \eta_0(T - T_0)^{-\gamma}$ with $\eta_0 = 137.46 \mu\text{Pa s}$, $T_s = 225.9151 \text{ K}$ and $\gamma = 1.6383$ (resp. $\eta_0 = 132.12 \mu\text{Pa s}$, $T_s = 230.9681 \text{ K}$ and $\gamma = 1.7061$).

T (K)	H ₂ O		D ₂ O	
	η (mPa s)	Relative uncertainty (%)	η (mPa s)	Relative uncertainty (%)
240.15	12.74	2.1		
241.15	11.40	2.1		
242.15	10.27	2.0		
243.15	9.31	1.9		
243.70			18.55	7.0
244.15	8.49	1.9	17.49	7.0
245.15	7.78	1.8	15.44	7.0
246.15	7.16	1.8	13.74	7.0
247.15	6.62	1.8	12.32	7.0
248.15	6.14	1.7	11.13	7.0
249.15	5.71	1.7	10.10	7.0
250.15	5.33	1.7	9.22	4.0
251.15	4.99	1.7	8.45	4.0
252.15	4.68	1.7	7.78	4.0
253.15	4.40	1.7	7.20	4.0
254.15	4.15	1.7	6.67	4.0
255.15	3.92	1.6	6.21	3.0
256.15	3.71	1.6	5.80	3.0
257.15	3.52	1.6	5.42	3.0
258.15	3.34	1.6	5.09	3.0
259.15	3.18	1.6	4.78	3.0
260.15	3.03	1.6	4.51	2.0
261.15	2.89	1.6	4.25	2.0
262.15	2.76	1.6	4.02	2.0
263.15	2.64	1.6	3.81	2.0
264.15	2.52	1.6	3.62	2.0
265.15	2.42	1.6	3.44	2.0
266.15	2.32	1.6	3.28	2.0
267.15	2.23	1.6	3.12	2.0
268.15	2.14	1.6	2.98	2.0
269.15	2.06	1.6	2.85	2.0
270.15	1.99	1.6	2.73	2.0
271.15	1.92	1.6	2.61	2.0
272.15	1.85	1.6	2.50	2.0
273.15	1.79	1.6	2.40	2.0
274.15	1.73	1.6	2.31	2.0
275.15	1.67	1.6	2.22	2.0
276.15	1.61	1.6	2.14	2.0
277.15	1.56	1.6	2.06	2.0
278.15	1.51	1.6	1.99	2.0
279.15	1.47	1.6	1.92	2.0
280.15	1.42	1.6	1.85	2.0
281.15	1.38	1.6	1.79	2.0
282.15	1.34	1.6	1.73	2.0
283.15	1.30	1.6	1.67	2.0
284.15	1.27	1.6	1.62	2.0
285.15	1.23	1.6	1.57	2.0
286.15	1.20	1.6	1.52	2.0
287.15	1.17	1.6	1.47	2.0
288.15	1.14	1.6	1.43	2.0
289.15	1.11	1.6	1.39	2.0
290.15	1.08	1.5	1.35	2.0
291.15	1.05	1.5	1.31	2.0
292.15	1.03	1.5	1.27	2.0
293.15	1.00	1.5	1.24	2.0

Shear viscosity and Stokes-Einstein violation in supercooled light and heavy water Supplemental Material

P. Ragueneau, F. Caupin and B. Issenmann*

Institut Lumière Matière, Université de Lyon, Université Claude Bernard Lyon 1, CNRS, F-69622, Villeurbanne, France

(Dated: March 14, 2022)

I. REORIENTATION OF WATER MOLECULES AND STOKES-EINSTEIN-DEBYE RELATION

The Debye model [1] which leads to the Stokes-Einstein-Debye (SED) relation assumes rotational Brownian motion of the reorienting object with a diffusion coefficient D_{rot} . This holds if the orientation changes as in a random walk, by small angular steps. With \vec{u} a unit vector describing the orientation, one defines the l -th order correlation function:

$$C_l(t) = \langle P_l[\vec{u}(0) \cdot \vec{u}(t)] \rangle, \quad (1)$$

where P_l is the l -th order Legendre polynomial and the angle brackets denote an ensemble average. The Debye theory predicts that the correlation functions decay exponentially [1]:

$$C_l(t) = \exp(-t/\tau_l) \quad \text{with} \quad \tau_l = \frac{1}{l(l+1)D_{\text{rot}}}. \quad (2)$$

The generalized Stokes-Einstein-Debye relation would thus be:

$$\frac{\eta}{l(l+1)T\tau_l} = \text{cst}, \quad (3)$$

with the same constant for all values of l .

NMR gives access to the integral rotational correlation time [2]:

$$\tau_\theta = \int_0^{+\infty} C_2(t) dt, \quad (4)$$

which is the quantity we consider in the present work. In the case of a Debye process, the rotational diffusion coefficient would thus be $D_{\text{rot}} = 1/(6\tau_\theta)$. Unfortunately, this simple picture does not apply to reorientation in water. Simulations have shown that a water molecule reorients by large-amplitude angular jumps [3], although the jump angle and the detailed description of the process vary among authors [2, 3]. The rotating water molecule breaks a hydrogen bond with an over-coordinated neighbor in its first shell, to form another bond with an under-coordinated neighbor in its second shell. Therefore, the NMR data should not be interpreted in terms of D_{rot} .

Recent simulations with the TIP4P/2005 water model have investigated how Eq. 3 is violated [4]. It was found that $\eta/(T\tau_l)$ increases when the temperature decreases, and behaves differently for different l . The dependence on the degree of Legendre polynomials led the authors to conclude that the SED violation is spurious. Nevertheless, it is remarkable that, for a given l , these simulations find $\eta/(T\tau_l)$ to be nearly temperature independent above 250 K. This is consistent with what is experimentally observed for $\eta/(T\tau_\theta)$. Therefore, while the Debye model is not applicable to the processes governing molecular reorientation in water, the SED relation remains a useful equation to assess the scaling between the experimentally accessible quantities, η and τ_θ .

* frederic.caupin@univ-lyon1.fr, bruno.issenmann@univ-lyon1.fr

II. TABLES

TABLE I: Raw values of the viscosity of H₂O

run number	T (K)	η (mPas)									
1	293.15	1.01	1.00	1.00	1.00	0.99	1.01				
	250.51	5.12	5.21	5.17							
2	293.15	1.01	1.00	1.00	1.01	1.00	1.02	1.01	0.99	0.98	
	250.51	5.28	5.24								
3	293.15	1.03	1.00	1.00	0.97	1.02	1.01	1.00	1.00	1.00	0.99
	254.41	4.10	4.10	4.15							
	250.57	5.31	5.24	5.16							
4	293.15	1.01	0.99	1.00	1.00	1.01	1.01	1.00	1.01	0.99	0.99
	254.36	4.13	4.05	4.12							
	252.43	4.38	4.41	4.63							
	250.51	5.19	4.91	5.17							
5	293.15	0.99	1.00	1.02	1.00	1.01	0.99	0.99	1.00	1.00	1.01
	254.56	3.98	3.92	3.96							
	252.66	4.62	4.52	4.60							
	250.75	5.12	5.12	5.19							
	248.85	5.70	5.86	5.76							
	246.94	6.62	6.56	6.56							
	245.03	7.94	8.11	7.60							
	244.08	8.53	8.34	8.68							
	243.13	9.61	9.26	9.22							
	242.17	10.17	10.24	10.24							
6	293.15	0.99	1.01	1.00	1.00	1.01	1.00	1.00	0.99	1.00	1.00
	288.10	1.14	1.13	1.13							
	283.31	1.31	1.29	1.33							
	278.52	1.51	1.50	1.51							
	273.72	1.75	1.78	1.78							
	268.93	2.09	2.11	2.10							
	264.14	2.54	2.59	2.62							

TABLE II: Raw values of the viscosity of H₂O–D₂O mixtures

run number	x_{D_2O} (%)	T (K)	η (mPa s)									
1	93.39	293.15	1.25	1.23	1.24	1.22	1.24	1.22	1.22	1.23	1.23	1.24
		278.47	1.92	1.92	1.91							
		273.63	2.30	2.31	2.29							
		268.80	2.81	2.81	2.83							
		263.97	3.61	3.59	3.58							
		259.14	4.71	4.71	4.72							
		256.24	5.67	5.66	5.62							
		254.30	6.45	6.47	6.53							
		252.37	7.34	7.48	7.58							
		251.40	8.13	8.05	8.11							
		250.44	8.71	8.87	8.75							
		249.47	9.53	9.53	9.69							
		248.50	10.74	10.63	10.49							
		247.54	11.37	11.23	11.69							
		246.57	12.92	13.14	12.88							
		246.09	13.62	13.51	13.74							
		245.61	14.48	14.35	14.62							
245.12	15.20	15.12	15.48									
244.64	16.15	16.41	16.39									
244.16	17.34	16.94	17.25									
243.67	18.07											
2	92.82	293.15	1.21	1.24	1.23	1.24	1.23	1.23	1.25	1.23	1.22	1.22
		278.44	1.92	1.91	1.96							
		273.63	2.27	2.30	2.32							
		264.02	3.54	3.51	3.51							
		254.41	6.28	6.33	6.42							

TABLE II: Raw values of the viscosity of H₂O–D₂O mixtures

run number	x_{D_2O} (%)	T (K)	η (mPas)									
3	91.71	293.15	1.23	1.23	1.22	1.23	1.22	1.22	1.22	1.24	1.23	1.23
		278.38	1.94	1.94	1.90							
		273.63	2.31	2.30	2.30							
		264.12	3.50	3.51	3.54							
		254.61	6.33	6.38	6.35							
		249.86	9.52	9.39	9.48							
		248.90	10.29	10.37	10.42							
		247.95	11.55	11.40								
		247.48	11.98	12.19	12.22							
		247.00	12.94	12.91	12.70							
		246.53	13.54	13.58								
		246.05	14.47	14.17	14.24							
		245.58	14.97	14.97	14.86							
		245.10	16.09	16.17	15.94							
244.63	17.09	16.90										
4	60.45	293.15	1.15	1.17	1.15	1.14	1.14	1.15	1.14	1.16	1.16	1.14
		278.42	1.79	1.77	1.78							
		268.84	2.57	2.51								
		264.04	3.15	3.14	3.21							
		259.25	4.09	4.06	3.89							
		256.37	4.81	4.83	4.85							
		254.46	5.44	5.44	5.42							
		252.54	6.20	6.13	6.23							
		250.62	7.17	7.20	7.20							
		248.71	8.56	8.44	8.45							
		247.75	9.16	9.30	9.36							
5	86.76	293.15	1.22	1.20	1.23	1.21	1.21	1.21	1.22	1.20	1.22	1.21
		283.19	1.60	1.64	1.60							
		278.41	1.88	1.89	1.89							
		273.63	2.28	2.28								
		268.85	2.73	2.72	2.74							
		264.07	3.44	3.47	3.44							
		259.29	4.48	4.52	4.52							
		256.42	5.39	5.39	5.36							
		254.51	6.10	6.16	6.18							
		252.60	7.07	7.07								
		250.68	8.45	8.39	8.47							

TABLE II: Raw values of the viscosity of H₂O–D₂O mixtures

run number	$x_{\text{D}_2\text{O}}$ (%)	T (K)	η (mPa s)									
9	49.96	293.15	1.12	1.12	1.13	1.12	1.14	1.13	1.12	1.12	1.13	1.11
		278.58	1.72	1.74								
		269.05	2.43	2.49	2.47							
		264.28	3.09	3.13	3.03							
		259.52	4.02	3.91	4.04							
		256.66	4.58									
		254.75	5.25	5.19	5.06							
		252.84	6.04	5.83	5.96							
		250.94	6.77									
10	47.46	293.15	1.14	1.15	1.14	1.11	1.13	1.12	1.08	1.09	1.11	1.11
		278.68	1.69	1.69	1.68							
		269.15	2.41	2.38	2.40							
		264.38	2.95	2.96	2.94							
		259.61	3.81	3.78	3.79							
		256.75	4.47	4.53	4.49							
		254.84	5.00	4.92	5.02							
		252.94	5.59	5.64	5.52							
		251.03	6.50	6.47	6.66							
		249.12	7.51	7.49	7.53							
		248.17	8.18	8.12	8.25							
		247.22	8.90	8.87	8.74							
		246.26	9.61	9.61	9.58							
		245.31	10.63	10.60	10.48							
244.36	11.75											

- [1] P. J. W. Debye, *Polar Molecules* (Dover Publications, New York, 1929).
- [2] J. Qvist, C. Mattea, E. P. Sunde, and B. Halle, Rotational dynamics in supercooled water from nuclear spin relaxation and molecular simulations, *J. Chem. Phys.* **136**, 204505 (2012).
- [3] D. Laage and J. T. Hynes, A Molecular Jump Mechanism of

- Water Reorientation, *Science* **311**, 832 (2006).
- [4] T. Kawasaki and K. Kim, Spurious violation of the Stokes–Einstein–Debye relation in supercooled water, *Sci Rep* **9**, 8118 (2019).